



ChemComm

Photochemistry of Carbon Nitrides and Heptazine Derivatives

Journal:	<i>ChemComm</i>
Manuscript ID	CC-FEA-05-2021-002745.R1
Article Type:	Feature Article

SCHOLARONE™
Manuscripts

Photochemistry of Carbon Nitrides and Heptazine

Derivatives

Doyk Hwang[†] and Cody W. Schlenker^{†,‡,†*}

[†]Department of Chemistry, University of Washington, Seattle, Washington 98195, United States

[‡]Molecular Engineering & Sciences Institute, University of Washington, Seattle, Washington 98195-1652, United States

^{†*}Clean Energy Institute, University of Washington, Seattle, Washington 98195-1653, United States

Abstract

We explore photochemistry of polymeric carbon nitride (C_3N_4), an archetypal organic photocatalyst, and derivatives of its structural monomer unit, heptazine (Hz). Through spectroscopic studies and computational analysis, we have observed that Hz derivatives can engage in non-innocent hydrogen bonding interactions with hydroxylic species. The photochemistry of these complexes is influenced by intermolecular $n\pi^*/\pi\pi^*$ mixing of non-bonding orbitals of each component and the relative energy of intermolecular charge-transfer (CT) states. Coupling of the former to the latter appears to facilitate proton-coupled electron transfer (PCET), resulting in biradical products. We have also observed that Hz derivatives exhibit an extremely rare inverted singlet/triplet energy splitting (ΔE_{ST}). In violation of Hund's multiplicity rules, the lowest energy singlet (S_1) is stabilized relative to the lowest triplet (T_1) electronic excited state. Exploiting this unique inverted ΔE_{ST} character has obvious implications for transformational discoveries in solid-state OLED lighting and photovoltaics. Harnessing this inverted ΔE_{ST} , paired with light-driven

intermolecular PCET reactions, may enable molecular transformations relevant for applications ranging from solar energy storage to new classes of non-triplet photoredox catalysts for pharmaceutical development. To this end, we have explored the possibility of optically controlling the photochemistry of Hz derivatives using ultrafast pump-push-probe spectroscopy. In this case, the excited state branching ratios among locally excited states of the chromophore and the reactive intermolecular CT state can be manipulated with an appropriate secondary “push” excitation pulse. These results indicate that we can predictively redirect chemical reactivity with light in this system, which is an avidly sought achievement in the field of photochemistry. Looking forward, we anticipate future opportunities for controlling heptazine photochemistry, including manipulating PCET reactivity with a diverse array of substrates and optically delivering reducing equivalents with, for example, water as a partial source of electrons and protons. Furthermore, we wholly expect that, over the next decade, materials such as Hz derivatives, that exhibit inverted ΔE_{ST} character, will spawn a significant new research effort in the field of thin-film optoelectronics, where controlling recombination via triplet excitonic states can play a critical role in determining device performance.

Introduction

An immense research effort has been expended to understand fundamental photochemical processes involving organic chromophores. On the one hand, insights gained from such studies can be of potential relevance for sustainable energy technologies, such as solar energy storage,¹⁻⁴ on the other, they can aid in developing preparative photoredox catalysts for chemical synthesis.⁵⁻⁹ While the sun has the capacity to provide ample energy to satiate immediate and future global power demands, its intermittency compels improvements in the overall cost, efficiency, and scalability of solar capture, conversion, and storage strategies.^{10, 11} Nevertheless, catalytically driving chemical reactions to store solar energy remains a challenging problem and an increasingly attractive goal.¹² There are numerous areas of reaction chemistry that would be desirable to drive with light, most prominent among these is arguably the splitting of water to generate hydrogen and oxygen.¹³⁻¹⁷ Other potential applications, may focus on photocatalytically generating, otherwise elusive, high-energy intermediates, such as amidyl radicals for synthesizing pharmaceuticals and other value-added products,^{6, 18} or reactive oxygen species for remediating polluted water.^{19, 20} These processes often involve complex kinetic barriers, which can, in principle, be traversed with PCET steps that require the coordinated motion of multiple electrons and multiple protons.²¹⁻²⁵ Much of the fundamental kinetics of these subtle and highly complex photochemical systems remain poorly understood and difficult to control. One common case involves the hydrogen and oxygen evolution reactions, where a murky understanding of the reaction kinetics appears to have stunted progress toward development and technological implementation of viable photocatalytic systems utilizing solar radiation.^{13, 16, 26}

Various strategies for tackling the water splitting problem exist, from conventional photovoltaic-electrolysis (PV-E) to photoelectrochemical (PEC) cells and photocatalyst suspensions.²⁷ While a suspension-based approach seems conceptually simple, the PV-E and PEC approaches enjoy substantial advantages for immediate implementation, including well-developed knowledge and infrastructure from existing technology. Practical solar-to-hydrogen (STH) efficiency limits for these more established

technologies have been estimated to be roughly 32% at 1 Sun irradiation.²⁸ Devices with STH efficiencies approaching these limits have been demonstrated at laboratory scale with PV-E²⁹ architectures. Similarly, devices based on PEC³⁰ architectures with STH efficiencies approaching the thermodynamic limit for a particular bandgap have also been demonstrated. However, technoeconomic analysis suggests that the levelized cost of hydrogen (LCH) produced by panel-based PV-E would be roughly three to five times higher than that predicted for photocatalytic systems and, indeed, uncompetitive against production from fossil sources.^{12, 31} As an alternative, some have postulated that suspension-based approaches with photocatalytic particles could potentially benefit from industrial plant designs with completely new form factors, with the potential to produce hydrogen at costs closer to current market prices.³¹ However, there are far more technological and scientific unknowns, not to mention market risks, associated with such approaches.^{12, 32} Not least of these is the obvious practical challenge of separating H₂ and O₂ products. Nevertheless, there have been numerous attempts to develop novel, efficient, inexpensive, and robust photocatalyst materials for the purpose of driving solar water splitting. These have ranged from semiconductor nanoparticles^{33, 34} to organic-based and polymeric photocatalysts.³⁵⁻³⁷ The perceived potential for low-cost and scalability has recently made organic photocatalysts an attractive platform. However, the challenges and uncertainties noted above for photocatalytic systems imply that, on some level, the value of such demonstrations may ultimately be rooted less in their direct technological significance and more in the fundamental insight that may be gleaned from these photochemical and electrochemical reactivity studies. Nevertheless, such new insight may foster new light-driven reaction chemistries or even hybrid energy storage devices, such as surface functionalized photoactive electrodes with heightened activity. For example, light-driven accumulation of two redox equivalents on surface-bound arylamines has recently been demonstrated on functionalized TiO₂ particles.³⁸ Given that it has long been recognized that such bipolaronic states form readily in many organic semiconductors,³⁹⁻⁴² it seems plausible that surface-bound systems capable of exploiting the accumulation of multiple redox equivalents may be of general significance to photocatalysis.

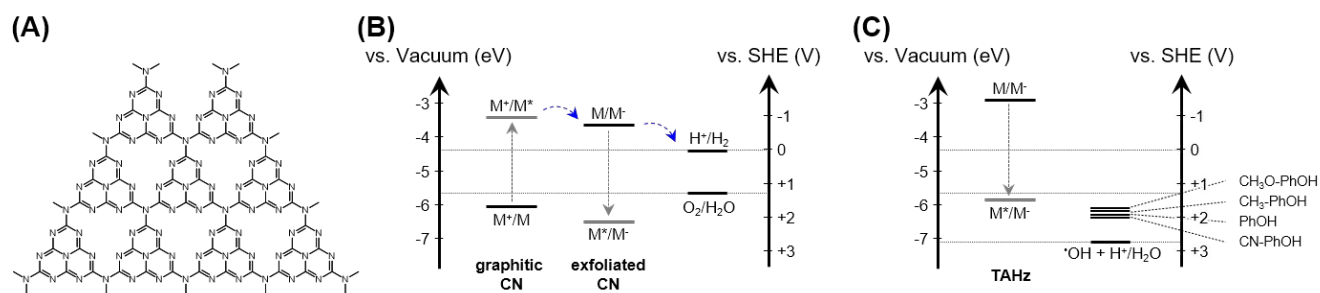


Figure 1 (A) Idealized molecular structure of graphitic Carbon Nitride (g-C₃N₄). (B) Experimentally measured redox potential and calculated excited-state redox potential from optical gap of g-C₃N₄, exfoliated C₃N₄, and (C) the monomeric Hz derivative 2,5,8-tris(4-methoxyphenyl)-1,3,4,6,7,9,9b-heptaazaphenalene (TAHz). Oxidation potential of g-C₃N₄ and reduction potential of exfoliated C₃N₄ and TAHz are measured by cyclic voltammetry (CV) with FTO working electrode, Ag/AgCl reference electrode, and Pt counter electrode. For g-C₃N₄ and exfoliated C₃N₄, CV was performed in sodium hydroxide (0.5 M, aq) with C₃N₄/nafion matrix coated FTO electrode. For TAHz, CV was performed with 475 μM TAHz in THF with 250 mM TABPF₆. Excited state redox potential was calculated with optical gap (S₀-S₁) determined from absorption and photoluminescence spectroscopy. For reference, half-reaction redox potentials of 2H⁺(aq)|H₂(g), O₂(g)+4H⁺(aq)|H₂O(l), [•]OH(aq)+H⁺(aq)|H₂O(l), and R-PhOH⁺|R-PhOH (in acetonitrile) are presented. Blue dashed arrows in (B) represent a viable electron transfer cascade pathway from photoexcited graphitic C₃N₄ to aqueous hydronium ion, resulting in H₂ evolution (see below). Adapted with permission from Ref. 102 and 107. Copyright 2017 and 2020 American Chemical Society.

One specific motivating factor behind a relatively intense recent research effort focused on organic-based materials for photocatalysis stems from the development of various polymeric carbon nitride (C₃N₄) materials over the past decade.⁴³⁻⁴⁹ Polymeric C₃N₄ exists in multiple forms, including poly-triazines and poly-heptazines; among those compositions, the most commonly studied subject is arguably graphitic C₃N₄ (g-C₃N₄), comprising two dimensional sheets of heptazine (Hz) units (**Figure 1A**).⁵⁰ The g-C₃N₄ variant has several desirable characteristics, including facile synthesis from common precursors and comparatively robust photochemical stability. It has also been shown that g-C₃N₄ has photocatalytic activity toward various reactions, ranging from water splitting and hydrogen evolution⁵¹ to carbon dioxide reduction,⁵² degradation of chemical pollutants,⁵³ and olefin hydroamidation.^{54, 55} Numerous chemical modifications of g-C₃N₄ have been applied to explore its photocatalytic activity. For example, Zhu and coworker applied chemical exfoliation to bulk g-C₃N₄ and observed an increase in their H₂ production rate of ~2.6 times, which they attributed to increased surface area.⁵⁶ Lau et al. showed chemical modifications that introduced oxygen containing terminal groups improved hydrogen generation efficiency.⁵⁷ Other works have focused on modifying morphology,⁵⁸ changes in crystallinity,⁵⁹ fragmentation of g-C₃N₄,⁶⁰ and metal ion doping.⁶¹

Lotsch and coworkers have taken a synthetic approach to evaluating the activity of polymeric C_3N_4 variants, in conjunction with computational analysis and experimental characterization, including X-ray diffraction, IR and NMR spectroscopy, mass spectrometry, and electron microscopy. Their work suggested that specific functional groups, such as the cyanamide moiety, support higher catalytic activity, which they surmised was due to enhanced coordination with a Pt co-catalyst.^{57, 62} The same group has also noted that different counter cations may influence activity by modulating inter-plane stacking.⁶³ Durrant and coworkers have taken a spectroscopic approach, using steady-state and femtosecond time-resolved spectroscopy to study excited state dynamics in several g- C_3N_4 variants.⁶⁴ From these results, they concluded that photoinduced electron accumulation occurred in their cyanamide-functionalized materials when paired with an appropriate sacrificial electron donor.⁶⁵ The authors in that work noted a correlation between their observed kinetic spectroscopy measurements and redox reaction mechanisms, and concluded that excessive electron accumulation limits the H_2 production rate by accelerating charge recombination.⁶⁶ Antonietti and coworkers have surveyed a range of C_3N_4 morphologies and chemical functionalization. Modifications such as co-condensation and shortening interlayer distance,⁶⁷ introducing nanostructured geometries,⁶⁸ or increasing structural flexibility,⁶⁹ appear to increase the oscillator strength of formally symmetry-forbidden low-energy Hz transitions. Many other studies have focused on leveraging the symmetry-forbidden, weak $n\pi^*$ transition that extends into the visible region to improve the spectral response of C_3N_4 at longer wavelengths.⁷⁰⁻⁷³ Other groups have employed quantum chemical calculations, such as recent surface hopping and nonadiabatic quantum dynamics simulations,⁷⁴⁻⁷⁷ to evaluate plausible photochemical pathways for C_3N_4 photocatalysis.

However, the preponderance of previous work has focused on g- C_3N_4 materials in the context of their potential semiconductor photophysics, such as bandgap and exciton dynamics.⁷⁸⁻⁸² By comparison, analysis of catalytic activity of g- C_3N_4 based on its molecular monomers and their photochemical properties has received far less attention, with only a few reported results.^{62, 83-86} However, the ever-present structural

heterogeneity and diverse chemical composition of g-C₃N₄ materials makes it extremely difficult to conduct systematic analysis of their photoactivity. To the best of our knowledge, there have been no reports demonstrating pure ballistic charge transport in carbon nitrides. While charge generation, likely at interlayer defect sites, has been observed spectroscopically on rapid, sub-picosecond timescales, photon absorption appears to initially produce bound excitons in these materials. For example, based on detailed photoluminescence analysis, Merschjann and coworkers concluded that 2-D Hz-based C₃N₄ behave electronically as optical quasi-monomers, rather than classical wide band gap covalent crystalline semiconductors.⁸⁷ Domcke, Sobolewski and coworkers studied a molecular mechanism of C₃N₄ photocatalysis from ab initio computational analysis, suggesting that a photochemical reaction of the Hz moiety and water may be active in C₃N₄.⁸⁸ Contrast this with the photoinduced electron transfer processes that are widely studied for proton reduction by semiconductor photocatalysts. This analysis suggests that the language of local molecular orbital interactions may lead to fruitful mechanistic insight regarding the photochemical reactivity of g-C₃N₄. Nevertheless, a common lexicon to describe material properties can be a unifying force in a multidisciplinary arena. We adopt a nomenclature that we have discussed previously,⁸⁹⁻⁹¹ which is based on the oxidizing and reducing potentials of the ground or excited electronic states, rather than on the nature of their charge transport characteristics, be they band-like, hopping, or otherwise. Using this excited state potential framework, the driving force for photoinduced charge transfer of C₃N₄ can be compared against classic semiconductors, polymers, or molecules with minimal confusion.

Figure 1B and **1C** show ground and excited state redox potentials of g-C₃N₄, chemically exfoliated C₃N₄, and the anisole-functionalized Hz monomer derivative, TAHz, compared with redox potentials of the hydrogen or oxygen evolution and the one-electron oxidation reactions for various hydroxylic species.^{92, 93} Based upon the corresponding thermochemical landscape, one anticipates that, upon photoexcitation, bulk g-C₃N₄, chemically exfoliated C₃N₄ flakes, and TAHz could all be capable of photochemically generating hydrogen or oxygen from water. However, as shown in numerous previous research with C₃N₄ and other catalytic systems, there exist other aspects that are critical for determining the overall photocatalytic

efficiency.⁴⁶ One important, widely accepted bottleneck in the water splitting reaction is the kinetically-limited four-electron transfer process of oxygen evolution reaction.¹⁵⁻¹⁷ Alternatively, there has been significant interest recently in photocatalytically generating $\bullet\text{OH}$ or H_2O_2 , as well as using water as a source of electrons and protons for running photocatalytic reduction reactions.⁹⁴⁻⁹⁷

Pairing ultrafast spectroscopy measurements with *ab initio* quantum chemical calculations has recently revealed the role of H-bonding interactions as one critical element for supporting photoinduced intermolecular PCET reactions, resulting in homolytic O-H bond cleavage. Domcke, Sobolewski, and coworkers have explored H-bond formation of Hz monomers in g- C_3N_4 with water and excited state PCET processes resulting in water oxidation using *ab initio* calculations and compared these results with well-known N-heterocyclic molecules such as pyridine and triazine.^{85, 88} A similar PCET-induced water oxidation reaction was also observed by Zhang and coworkers from excited state nonadiabatic dynamics simulation showing ultrafast electron-driven proton transfer from water to Hz,⁷⁵ and also by Bande and coworkers from their excited state electron dynamics calculation with nitrogen-doped C_3N_4 -like graphene oxides.⁹⁸ Notably, these studies generally indicate that the traditional electrochemical potentials used to estimate reaction free energies such as those presented in **Figure 1B** and **1C**, for bulk g- C_3N_4 , chemically exfoliated C_3N_4 flakes, and a monomeric Hz derivative do not adequately represent the photochemical reactivity of the hydrogen bonded complex. Rather, one-electron water oxidation is facilitated through the PCET process and the thermodynamically favorable but kinetically cumbersome four-electron transfer process is avoided.^{84, 99, 100}

As we describe in this Feature Article, one of our goals has been to reveal new insight into the fundamental photochemistry of heptazine-based materials by spectroscopically examining the kinetics of the excited-state reaction chemistry in which they engage. Among several findings that our work has uncovered, the following are particularly noteworthy: 1) intermolecular hydrogen bonding interactions result in new excited states, which appear to serve as a gateway to hole transfer from hydroxylic species; 2) this hole transfer can be predictably controlled using tunable laser pulse sequences; 3) the intermolecular

hydrogen bonding interaction appears to influence excited state deformations of the chromophore, which may modulate these photon-driven reactions; and 4) the intriguing photophysical and photochemical behavior of heptazine derivatives is, in part, due to a rather unique inversion of its lowest-energy singlet and triplet excited states that results from a combination of spin polarization effects and the orthogonality of their HOMO and LUMO orbitals.

Mechanistic Study of Carbon Nitride Photocatalyst

I. Ultrafast Electron Transfer and Reactivity Enhancement in Polymeric Carbon Nitriles

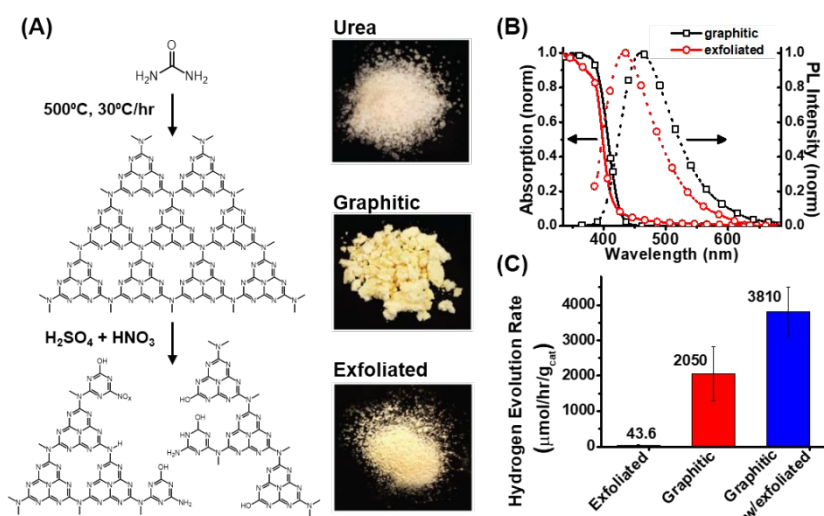


Figure 2 (A) Schematic diagram for synthesis of g-C₃N₄ from Urea and chemical exfoliation of g-C₃N₄ into exfoliated flakes. (B) Ground-state absorption (solid lines) and steady-state luminescence spectra (dotted lines) for 365-nm excitation of graphitic (black) and exfoliated (red) C₃N₄ suspensions in deionized water. (C) Hydrogen activity for exfoliated C₃N₄, g-C₃N₄ and a g-C₃N₄ suspension infused with 10% mass-loading of exfoliated C₃N₄ co-catalyst under 365-nm LED illumination (21 mW/cm²). Rates are for 2% Pt loading with 10% triethanolamine used as a sacrificial hole scavenger. Reprinted with permission from Ref. 102. Copyright 2017 American Chemical Society.

Among the numerous studies regarding the catalytic activity of g-C₃N₄ photocatalysts, several have found that specific chemical modifications of g-C₃N₄, including introducing defects¹⁰¹ or oxidative terminations⁵⁷ in bulk g-C₃N₄ enhance performance of photocatalysis. In particular, adding chemically exfoliated C₃N₄ flakes with more termination sites improves catalytic activity and hydrogen production rates of bulk g-C₃N₄ by ~2.3 times, even without a Pt co-catalyst.⁶⁰ Based on these experimental observations, our group initially focused on a heterogeneous g-C₃N₄ catalyst platform blended with exfoliated C₃N₄. This effort centered on revealing the underlying dynamic processes associated with this catalytic efficiency enhancement and clarifying the fundamental photocatalytic reaction mechanism of C₃N₄ catalysts. **Figure 2A** shows preparation routes for g-C₃N₄ and exfoliated C₃N₄.¹⁰² Briefly, g-C₃N₄ powder was treated with a highly-oxidizing mixture of sulfuric and nitric acids under ultrasonication and stirring. After 24 hours, the resulting

mixture was treated with deionized water and filtered through a 0.45 μm PVDF mesoporous membrane. This process introduced oxidized termination sites and also shortened the π -conjugation length of the resulting heptazine-based material. These properties were explored using the experimental characterization tools described below. Based upon results from our X-ray photoelectron spectroscopy (XPS), FT-IR spectroscopy, and X-ray diffraction studies, the exfoliated C_3N_4 evidently differs from the parent bulk material in that it possesses substantially more oxidized chain terminations than bulk $\text{g-C}_3\text{N}_4$, which may serve as photochemical reaction sites. However, X-ray diffraction indicates that some degree of periodicity among Hz units is still maintained following the exfoliation process.¹⁰² Consistent with the shorter π -conjugation length resulting from an increase in the number of chain terminations, exfoliated C_3N_4 exhibited a blue-shifted optical energy gap, observable in both the steady-state absorption and photoluminescence spectra (**Figure 2B**). The optical energy gap, combined with electrochemical characterization, allow us to consider the energy levels for charge transfer, shown in **Figure 1B**. These energy level estimates indicate that electron transfer from photoexcited $\text{g-C}_3\text{N}_4$ to our chemically exfoliated C_3N_4 material is an exergonic process. Interestingly, incorporating a small amount (10% by mass) of exfoliated C_3N_4 into a $\text{g-C}_3\text{N}_4$ suspension significantly enhances the catalytic activity of $\text{g-C}_3\text{N}_4$ (**Figure 2C**), this despite exfoliated C_3N_4 alone being virtually inactive toward H_2 production.

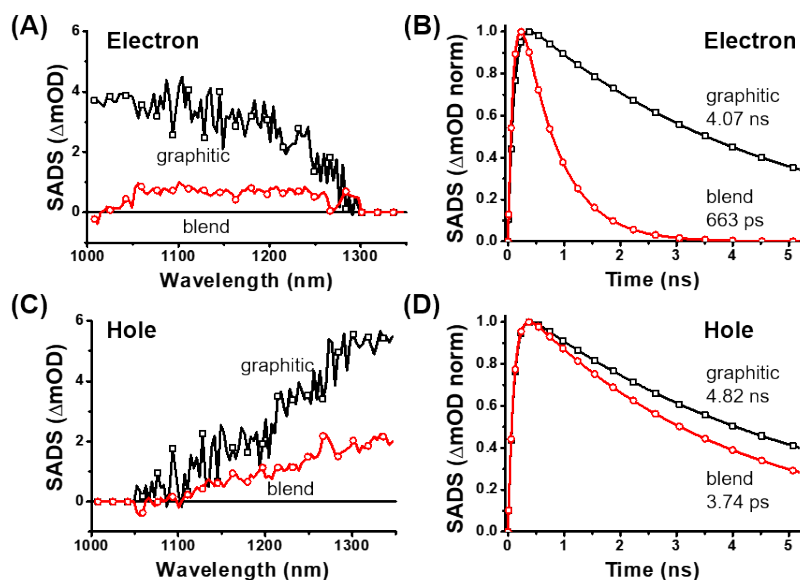


Figure 3 Global target analysis of the femtosecond transient absorption data for g-C₃N₄ and a mixture of g-C₃N₄ plus 10% exfoliated C₃N₄ by mass (“blend”) in deionized water. Species associated difference spectra (SADS), σ_e for the electron (A) and σ_h for the hole (C), correspond to the kinetics profiles in (B) and (D), respectively. The data used for this analysis were collected without platinum loading and in the absence of charge scavengers. Reprinted with permission from Ref. 102. Copyright 2017 American Chemical Society.

Photogenerated excitons and charge carriers, the primary participants in most photochemical and photophysical processes, are typically transferred on rapid timescales from femtoseconds to microseconds.¹⁰³ As a result, conventional steady-state characterization methods often fail to provide sufficient mechanistic information about the excited state species that drive photocatalytic reactions. Accordingly, we have utilized ultrafast spectroscopic techniques, including femtosecond transient absorption (TA) spectroscopy, in order to thoroughly probe photoinduced dynamics in the g-C₃N₄ mixed with exfoliated C₃N₄. As indicated in **Figure 3**, global target analysis reveals that two different species contribute to the overall TA signal in the NIR probe range of the spectra for the g-C₃N₄ and blend samples. In global target analysis, we assume that experimental TA data consists of the superposition of species-associated difference spectra (SADS), weighted by a time-dependent concentration profile for each contributing species.^{104, 105} By comparing each SADS from our TA experiments with differential absorption spectra from cathodic spectroelectrochemical measurements,¹⁰² we concluded that the two SADS recovered from our target analysis were attributable to photogenerated electrons and holes in g-C₃N₄, as shown in

Figure 3. This assignment was corroborated by control experiments wherein electron or hole scavengers were added to the sample.¹⁰²

As shown in **Figure 3**, adding exfoliated C_3N_4 flakes drastically quenches the photogenerated $g-C_3N_4$ electron signal but produces a negligible effect on the hole decay kinetics. The accelerated decay constant of photogenerated electron in $g-C_3N_4$ is about 660 ps, which is on the same order of diffusion-limited quenching. Since the concentration of exfoliated C_3N_4 is substantially lower than $g-C_3N_4$ in the blend sample (~10% by mass), these results indicate that the electrons initially photogenerated in $g-C_3N_4$ are rapidly transferred to exfoliated C_3N_4 and the catalytic enhancement primarily occurs at the exfoliated C_3N_4 containing the oxidized chain termination sites. This hypothesis is also supported by prior experimental observations⁶⁰ that adding small amounts of exfoliated C_3N_4 flakes drastically enhances catalytic activity of bulk $g-C_3N_4$. The enhanced catalytic activity upon adding chemically exfoliated $g-C_3N_4$ particles is consistent with previous structure-activity studies of carbon nitrides. These results indicated that introducing structural defects and increasing the number of chemically activated $g-C_3N_4$ chain termination sites, such as highly oxidized terminal groups, improves catalytic activity.¹⁰⁶⁻¹⁰⁹ Based on these findings, we anticipated that heptazine oligomers or even monomers, may serve as viable photocatalysts and may exhibit compelling photochemistry in their own right.¹¹⁰

II. Proton-Coupled Electron Transfer in Monomeric Heptazine Photocatalysts

The monomeric heptazine unit of g-C₃N₄ (**Figure 1**), has garnered significant research interest from the energy storage community.^{62, 88, 111, 112} This is, in part, due to the observations described above suggesting that exfoliated C₃N₄ can improve catalytic activity, but also from a fundamental standpoint as a testbed to better understand photon-driven chemical transformations, such as H-atom abstraction, in greater detail.⁸⁴ We synthesized TAHz using Friedel-Crafts chemistry as a stable, well-defined, model Hz derivative (**Figure 4**). We investigated its photophysical and photochemical properties in the presence of various hydroxylic compounds that are capable of hydrogen bonding with the nitrogen atoms on the perimeter of the heptazine core.¹¹³

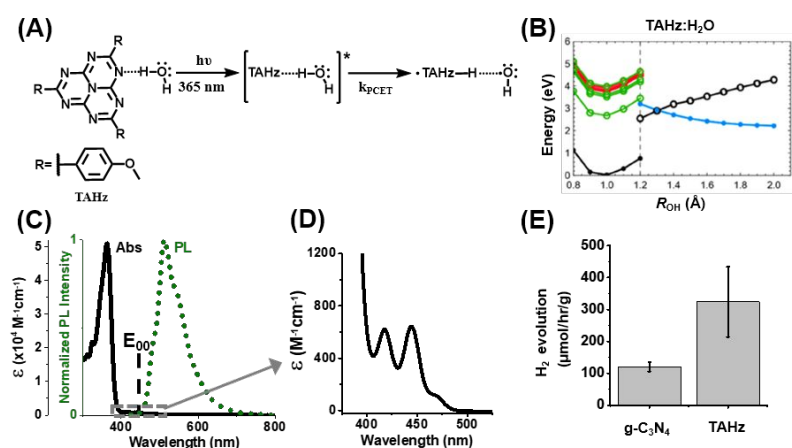


Figure 4 (A) Molecular structure of TAHz and proposed mechanism of PCET reaction with water. (B) *Ab initio* potential energy profiles of relaxed scans for the H-atom transfer reaction from water to TAHz. For $R_{OH} < 1.2 \text{ \AA}$, electronic ground state (black) was optimized, while for $R_{OH} > 1.2 \text{ \AA}$ the charge-transfer state (blue) was optimized. $\pi\pi^*$ states are shown in green, $n\pi^*$ states are shown in red. (C) Absorption and photoluminescence spectrum of TAHz in toluene (33 μM). (D) Absorption spectrum of weakly allowed transitions around 400 ~ 500 nm below bright $\pi\pi^*$ transition at 365 nm. (E) H₂ evolution rate for 3 mg TAHz, 15 mL of H₂O, 1.5 mL of triethanolamine, and 2 wt % Pt under 5 mW/cm², 365 nm LED illumination. H₂ activity of bulk g-C₃N₄ under identical conditions included for reference. Reprinted with permission from Ref. 113.

Copyright 2018 American Chemical Society.

Figure 4A depicts one potential hydrogen bonding motif between heptazine derivatives and water via the peripheral nitrogen atoms of the heptazine rings. This hydrogen bonding interaction has been predicted by *ab initio* quantum chemical calculations to help facilitate intermolecular PCET reactions from H₂O to TAHz, leading to TAHz-H[•] and •OH biradical products.⁸⁸ These theory-based results suggest that heptazine hydrogen bonding interactions with hydroxylic species, such as water, result in intermolecular complexes

wherein new excited states with charge-transfer (CT) character from the Hz core to the oxygen p-orbital are formed. These intermolecular electronic states are distinct from the local $\pi\pi^*$ and $n\pi^*$ excited states associated with the isolated chromophore. The trace marked with blue filled circles in the right portion of the energy diagram in **Figure 4B** illustrates that these CT states become energetically stabilized along the H-atom transfer coordinate. They can be regarded as a photochemical reaction pathway. Thus, excitation into the CT state can engender a PCET reaction, breaking the chemical bond between hydrogen and oxygen and transferring the H atom (electron + proton) to the heptazine core. In the subsequent sections of this Feature Article, we will outline a number of experimental observations reported by our group that are consistent with the theoretical framework described above for the photochemical reactivity of heptazine derivatives.

Electronic excited states of TAHz in the near UV to visible wavelength range mainly consist of an exceptionally bright, high-energy $\pi\pi^*$ state and a low-lying, symmetry-forbidden $\pi\pi^*$ state, with contributions from dark $n\pi^*$ states of intermediate energy. From computational analysis, we attribute the intense absorption peak near 360 nm to the bright $\pi\pi^*$ transition, while the much weaker absorption signatures near 450 nm and photoluminescence peak proximal to 510 nm are associated with a formally symmetry-forbidden $\pi\pi^*$ transition. In the absence of hydrogen bonding with an external H-atom donor, initial excitation of the TAHz through the bright $\pi\pi^*$ transition quickly results in nonradiative relaxation to the lowest dark $\pi\pi^*$ excited state, which then can emit green fluorescence. However, with H-atom donors such as water, photoexcitation can initiate PCET reactions, as well as H₂ evolution (**Figure 4E**). The PCET reaction was also probed by a drastic quenching of fluorescence lifetime of TAHz in water compared to that in toluene, and the $\cdot\text{OH}$ radical generation was detected by various methods, such as terephthalic acid adduct fluorescence¹¹³ and spin-trapping EPR.⁸⁴ Interestingly, we see an H₂ production rate per mass catalyst from TAHz that is roughly on par with bulk g-C₃N₄ under otherwise identical conditions.¹⁰²

In order to probe dynamics of the TAHz:H₂O complex and better understand the kinetics of this PCET reaction, we employed time-resolved PL (TR-PL) spectroscopy paired with global target analysis. While

the overall emission spectral line shapes in toluene and water appear to be somewhat similar, there are striking kinetic differences in the fluorescence that are revealed by analyzing the blue-edge (high-energy, short-wavelength region) of the emission envelope (**Figure 5A**). Comparing decay kinetics at short and long wavelengths of this signal showed that there exist at least two different emitting species for the TAHz in water case. By contrast, we only observe one single emitting species in toluene, which is attributable to the S_1 excited state of free TAHz. We were able to resolve two different emission spectra contributing to the TR-PL data of TAHz in water using global analysis. These results reveal a new high-energy emission spectrum with shorter average lifetime, in addition to the low-energy spectrum that is attributable to free TAHz.

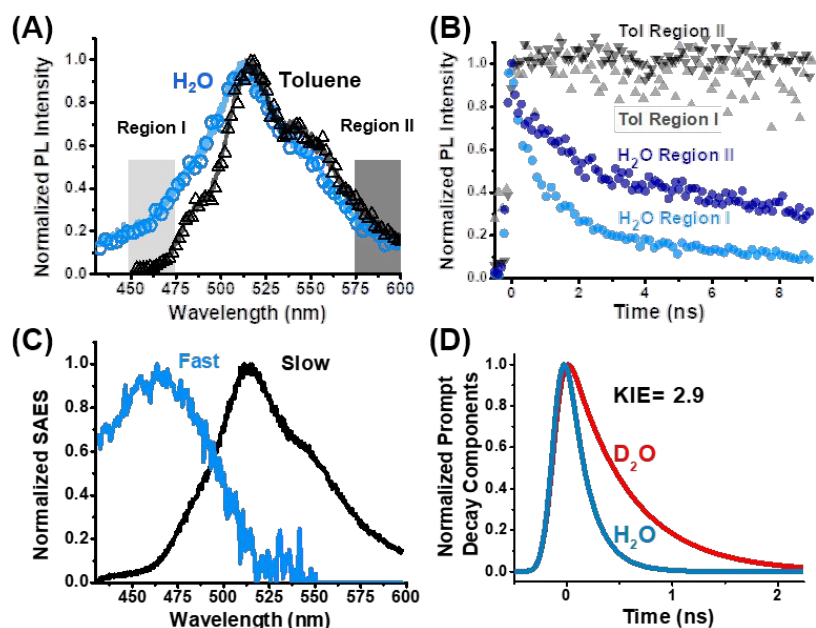


Figure 5 Time-resolved photoluminescence (TR-PL) of TAHz in water and toluene (365 nm, 100 fs pulse excitation). (A) PL spectra averaged over the first 500 ps after excitation. In water (blue), TAHz exhibit a new PL feature at higher photon energy (region I) compared to TAHz in toluene. Solid lines are globally fitted lines of the data (symbols). (B) PL kinetics traces of TAHz in water (blue) and toluene (black). In toluene, traces from region I and II exhibit identical monoexponential decay kinetics. Decay traces for TAHz in water are distinct from those of region I and II, suggesting two kinetically distinct emissive states exist. (C) Species-associated emission spectra (SAES) from global analysis of the TAHz in water PL exhibit two different spectral components, fast (blue) and slow (black). (D) The prompt decay components of the high-energy emitting species from global analysis for TAHz in D₂O (red) and H₂O (blue). The kinetic isotopic effect (KIE = 2.9), calculated from the lifetime ratio, is consistent with dynamic quenching of the high-energy emission by PCET. Adapted with permission from Ref. 113. Copyright 2018 American Chemical Society.

Since excited state PCET processes involve physical movement of a proton, one common way to characterize such a reaction is to deuterate the participating protic component, which, in many cases, can substantially decelerate the reaction kinetics.^{114, 115} When we changed the solvent from H₂O to D₂O, we observed a considerable kinetic isotope effect (KIE) in the PL lifetime of the high-energy emitting species, increasing by a factor of 2.9 (**Figure 5D**). This result is consistent with H-atom transfer quenching of the luminescence as a result of the PCET reaction. On the other hand, the low-energy emitting species did not exhibit a substantial KIE upon deuteration, as expected for free TAHz undergoing collisional quenching. These results indicate that TAHz can form hydrogen bonded complexes with water that undergo photon-driven PCET reactions, resulting in one-electron homolytic water oxidation reactions to generate biradical products, as well as liberating H₂. In this Feature Article, we cover two primary photoactivity modes for

heptazine-based photocatalysts. One operating by reducing a substrate (i.e., electron transfer to protons). The other operating by oxidizing a substrate (i.e., PCET from water to the chromophore). Sacrificial reducing agents, which are often used in consort with metal co-catalysts, preferentially steer the photocatalytic activity toward proton reduction, masking any underlying activity toward water oxidation. For example, photoexcited TAHz will oxidize pure water by abstracting hydrogen atom from it. However, we have shown that feeding photoexcited TAHz with triethanolamine as a sacrificial electron donor in an aqueous environment will cause TAHz to preferentially reduce protons instead.¹¹³ Results from Kang and coworkers indicate that a composite of metal-free polymeric g-C₃N₄ and carbon nanodots, without any sacrificial reducing agent, supports photocatalytic water splitting by a two-electron water oxidation pathway, generating H₂ and O₂ via a peroxide intermediate.¹¹⁶ More recent theory studies, employing tools such as nonadiabatic quantum dynamics simulations, have suggested that this overall water oxidation process is initiated by an excited-state PCET event that transfers an H-atom from water to the peripheral nitrogens in the heptazine ring of polymeric g-C₃N₄.^{76, 77} The substrate oxidation process described in those theoretical and experimental reports is consistent with the “PCET from substrate” reactivity that we observe for molecular heptazine derivatives, such as TAHz.^{75, 84} In the following sections, we focus on a model system to further explore the excited-state PCET reactivity of TAHz with functionalized phenols, to reveal more systematic control of molecular properties and a deeper understanding of the excited states involved.

Comprehensive Understanding of Photochemical Reactions in Model Heptazine Systems

I. Measurement and Manipulation of Molecular Properties with Substituted Phenol Substrates

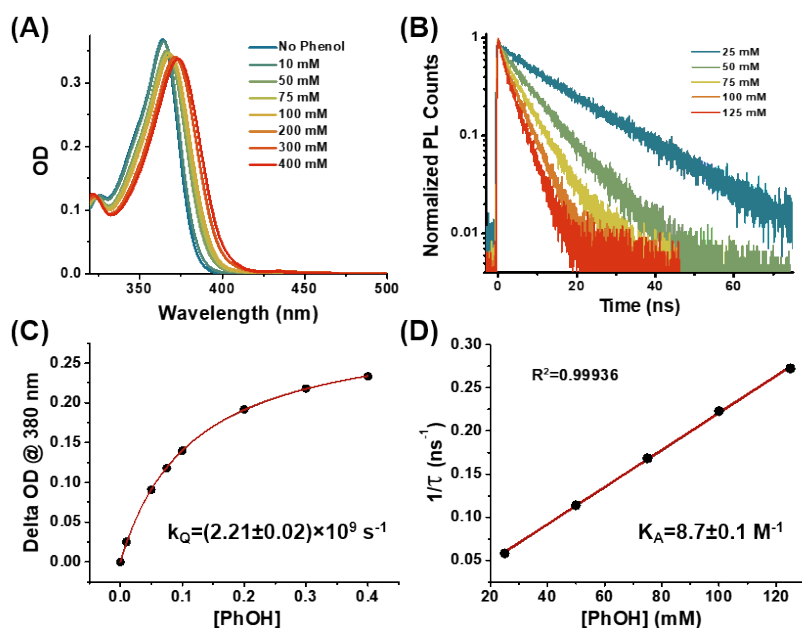
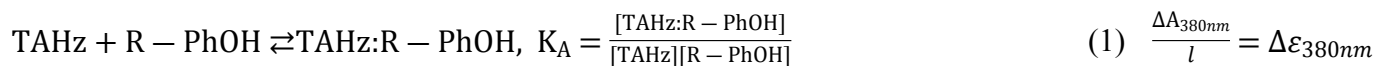


Figure 6 Evolution of photophysical properties as a function of PhOH concentrations for TAHz solutions in toluene. (A) absorption spectra. (B) photoluminescence lifetime. (C) association constant determination from absorption spectral change. (D) Stern-Volmer plot from photoluminescence lifetime change. Reprinted with permission from Ref. 93. Copyright 2019 American Chemical Society.

In order to gain further insights regarding the role of hydrogen bonding in the PCET reaction of molecular heptazine photocatalysts, we paired TAHz with para-substituted phenol substrates (R-PhOH) as a model system.⁹³ As shown in **Figure 6**, we observed that the bright $\pi\pi^*$ transition in the TAHz absorption spectrum red-shifts upon adding phenol due to the hydrogen bonding interaction. The fluorescence from the dark $\pi\pi^*$ excited state is strongly suppressed due to quenching of excited TAHz by the PCET reaction. The PCET reaction can also be monitored through generation of R-PhO \cdot radical products, probed by EPR spin trapping experiments.¹¹⁷ Based on first-order association equilibrium analysis of the absorption peak shift¹¹⁸ and Stern-Volmer analysis of the photoluminescence intensity and lifetime quenching,¹¹⁹ we were able to quantitatively evaluate some basic properties of the TAHz:R-PhOH photochemistry as follows:



$$\left(\frac{[\text{TAHz}]_0 + [\text{R} - \text{PhOH}]_0 + K_A^{-1}}{2} \right) \pm \sqrt{\left(\frac{[\text{TAHz}]_0 + [\text{R} - \text{PhOH}]_0 + K_A^{-1}}{2} \right)^2 - [\text{TAHz}]_0[\text{R} - \text{PhOH}]_0} \quad (2) \quad \frac{I_{\text{Fl}}^0}{I_{\text{Fl}}} = \frac{\tau_{\text{Fl}}^0}{\tau_{\text{Fl}}} = 1 + k_Q \tau_{\text{Fl}}^0$$

$[\text{R} - \text{PhOH}]_0$ (3) where K_A is the association constant of the ground state complex, $\Delta A_{380\text{nm}}$ is the absorbance change at a given wavelength (in this case, 380 nm), l is the path length of sample cuvette, $\Delta \epsilon_{380\text{nm}}$ is change of molar extinction coefficient between free TAHz and the TAHz:R-PhOH complex, $[\text{TAHz}]_0$ and $[\text{R-PhOH}]_0$ are the initial concentrations of each molecule, I_{Fl} and τ_{Fl} are the fluorescence intensity and lifetime of TAHz in phenol – toluene solution, I_{Fl}^0 and τ_{Fl}^0 are the intensity and lifetime of TAHz in pure toluene, and k_Q is the PL quenching constant. We also explored the possibility of multiple hydrogen bonds, due to many nitrogen atoms in the heptazine core, and were able to identify 1:1 and 1:2 hydrogen-bonded complexes of TAHz and phenol at a higher phenol concentration range (up to ~900 mM).¹²⁰ In following steady-state and time-resolved PL studies, we kept the concentration of R-PhOHs low

R	E_0 (R-PhOH ⁺ /R-PhOH) ^a	$\text{p}K_a$ R-PhOH ^b	k_Q ($\times 10^9 \text{ s}^{-1}$) TCSPC	k_Q ($\times 10^9 \text{ s}^{-1}$) PLQY	K_A (M^{-1})	S_1 KIE	R_{NH} (Å)	ΔE^\ddagger (eV)
CN	2.03	13.2	0.556 ± 0.05	0.53 ± 0.02	58 ± 3	1.9 ± 0.1	1.904	0.369
Cl	1.88	16.75	2.78 ± 0.03	2.785 ± 0.007	17.2 ± 0.3	1.36 ± 0.04	1.924	0.169
Br	1.86	16.36	2.73 ± 0.03	3.053 ± 0.009	19.1 ± 0.7	1.36 ± 0.05	1.923	0.177
H	1.88	18.0	2.21 ± 0.02	2.579 ± 0.004	8.7 ± 0.1	1.5 ± 0.1	1.937	0.167
CH ₃	1.79	18.9	4.21 ± 0.02	5.124 ± 0.007	8.9 ± 0.2	1.19 ± 0.04	1.940	0.093
OCH ₃	1.68	19.1	4.26 ± 0.03	5.218 ± 0.008	8.9 ± 0.4	1.06 ± 0.02	1.943	

^aversus SHE in acetonitrile.^{121, 122} ^bin DMSO.¹²³

Table 1 Chemical properties of 4-substituted phenols and their complexes with TAHz in toluene. E_0 (R-PhOH⁺/R-PhOH) is oxidation potential (versus SHE in acetonitrile). $\text{p}K_a$ values refer to R-PhOH species in DMSO solvent. k_Q TCSPC or k_Q PLQY are Stern-Volmer quenching constants calculated from photoluminescence lifetime or quantum yield measurements, respectively. K_A is an association constant from absorption measurement. S_1 kinetic isotope effect (KIE) values were calculated from the lifetime of TAHz PL with R-PhOH vs. R-PhOD. R_{NH} and ΔE^\ddagger are the hydrogen bonding distance and reaction barrier enough that the dominant hydrogen-bonded species are the 1:1 complexes. Parameters obtained from fitting, chemical properties of different R-PhOHs, calculated hydrogen bonding distances and PCET reaction barriers are presented in **Table 1**.

As shown in **Table 1**, we were able to manipulate the redox potential of the phenol substrates, and also modulate hydrogen bonding strength between TAHz and R-PhOH, by changing the functional group on the

para-substituted phenols.⁹³ Increasing electron donating strength of the functional group from 4-cyanophenol to 4-methoxyphenol, we observed the following trends in photochemical properties of TAHz:R-PhOH complexes: the association constant (K_A) decreases, while the PCET reaction rate increases, based on the Stern-Volmer quenching rate constant (k_Q). The decrease in K_A , consistent with the calculated hydrogen bonding strength (R_{NH} in **Table 1**), follows one's chemical intuition that stronger electron donating character of the functional group should result in a less polarized O-H group on the phenol moiety, which ultimately weakens the hydrogen bonding interaction. The increase in the PCET reaction rate that accompanies the larger thermodynamic driving force due to the decreased oxidation potential of R-PhOH also acts to suppress the reaction barrier under the conditions studies here, as described below.

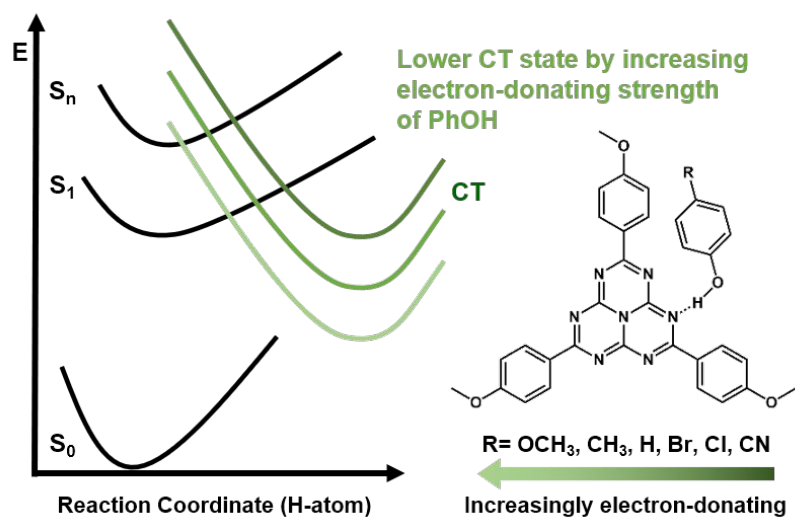


Figure 7 Schematic depiction of the proposed excited state landscape along the H-atom transfer coordinate from R-PhOH to TAHz. As proposed previously for the TAHz:H₂O complex, there exists a CT state in which an electron moves from the oxygen atom of PhOH to the heptazine core and can drive proton motion. Previous studies with TAHz:H₂O complex suggested the CT state is accessible from higher-lying bright excited states. We hypothesized that the energy curve of the CT state could be stabilized by adding electron-donating groups on the H-atom donor. In this study, we do this by using the series of R-PhOH derivatives depicted above. Reprinted with permission from Ref. 93. Copyright 2019 American Chemical Society.

Changing the oxidation potential of R-PhOH has additional implications for the PCET reaction dynamics.

Figure 7 shows the potential energy surface of TAHz:R-PhOH complex along the H atom transfer coordinate. Since molecular orbitals associated with dark $\pi\pi^*(S_1)$ and bright $\pi\pi^*(S_n)$ excited states are

localized on the Hz core and anisole moieties of TAHz, one might expect that the energetics of those locally excited states would be minimally affected by changing the R-group on R-PhOH. However, the CT state will be significantly affected upon changes in the oxidation potential of R-PhOH as in **Figure 7**. This change in the excited state energy landscape not only tunes the thermodynamic driving force for the PCET reaction, but also the reaction barrier from the local excited state to the charge-transfer state, ΔE^\ddagger .

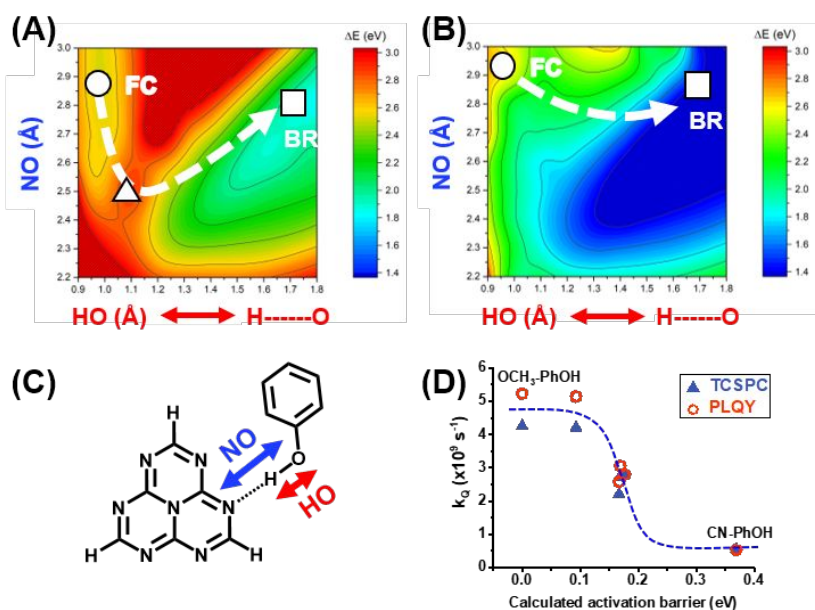


Figure 8 2D relaxed potential energy surface of the S_1 excited state of the (A) Hz:PhOH complex and (B) Hz:MeOPhOH complex computed at the ADC(2) (second-order algebraic diagrammatic construction) level. The reaction coordinates are the OH bond length of PhOH and the distance between the O-atom of PhOH and N-atom of Hz, see (C). The circle designates the energy minimum of the LE state in the FC region. The square indicates the equilibrium geometry of the HzH \cdots PhO \cdot biradical (BR) formed by H-atom transfer. A saddle point (marked by the triangle) separates the two energy minima. (D) Correlation between the calculated activation barrier and the excited state quenching rate constants, determined by photoluminescence quantum yield (PLQY; red open circles) and lifetime (TCSPC; blue triangles). Overall, we see a significant increase in the excited-state quenching rate as the phenol substituent becomes more electron-donating, becoming saturated at MeOPhOH case. Dashed line is a guide for the eye. Adapted with permission from Ref. 93. Copyright 2019 American Chemical Society.

Excited-state reaction barriers were quantitatively evaluated computationally based on relaxed two-dimensional potential energy surfaces, calculated at the lowest energy singlet excited state of the Hz:R-

PhOH complex along the H atom transfer coordinate and intermolecular distance between Hz and R-PhOH, as shown in **Figure 8**.⁹³ Consistent with the schematic diagram in **Figure 7**, the Hz:R-PhOH complex at the S_1 state must traverse from the Franck-Condon geometry to the biradical product geometry through a saddle point, which is energetically higher than Franck-Condon geometry by the reaction barrier height, ΔE^\ddagger . Calculated ΔE^\ddagger values for different R-PhOH species are shown in **Table 1**. As expected, ΔE^\ddagger becomes lower as the R-group becomes more electron donating; eventually, at the 4-methoxyphenol limit, the reaction barrier disappears and PCET becomes barrierless (**Figure 8B**). Experimentally, we probed this trend in the activation barrier using Stern-Volmer quenching analysis to assess the rate constants (**Figure 8D**) and kinetic isotope effects (KIE) on photoluminescence lifetime between R-PhOH vs. R-PhOD (**Table 1**). By changing the R-group from cyano to methyl, ΔE^\ddagger becomes smaller and the PCET reaction becomes more rapid. Thus, k_Q increases and KIE decreases. At the 4-methoxyphenol limit, the reaction barrier is eliminated, k_Q saturates, and KIE nearly vanishes accordingly.

These experimental trends and computational results revealed a distinct control knob for manipulating reactivity of Hz photocatalysts: the redox potential difference between catalyst and substrate. In our case, the substrate side of the catalysis system, R-PhOH, was modified. However, one could envision reversing this approach by changing the redox potential of the Hz catalysts by modifying the pendant groups attached to the Hz core to be stronger electron withdrawing moieties. Another interesting result is the possibility of fine-tuning the reactivity based upon the hydrogen bonding environment. If we compare the 4-chlorophenol to the phenol case in **Table 1**, the hydrogen bond formation is stronger and the PCET reaction is faster for 4-chlorophenol, while the oxidation potentials for both cases are almost identical. Since the photocatalytic reaction of the TAHz:R-PhOH complex is a combination of electron and proton transfer processes, we suspected that hydrogen bonding interactions also play a considerable role in addition to the primary role that the electrochemical redox potential appears to play. To this end, in the next section, we explore the influence that hydrogen bonding appears to exert on the excited state properties of these intermolecular complexes.

II. The Influence of Hydrogen Bonding on Hz Excited State Geometry

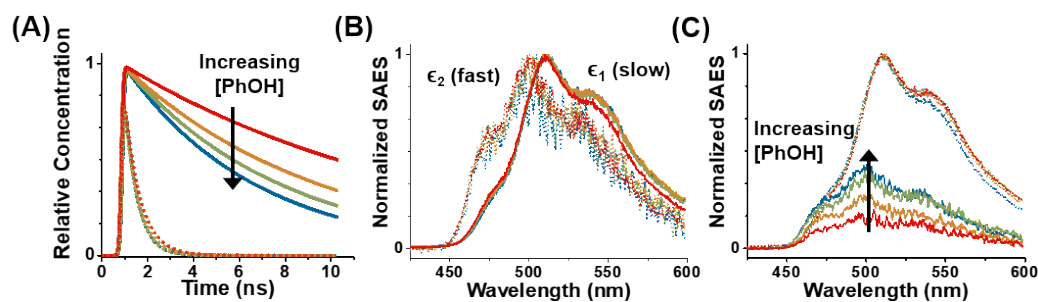


Figure 9 Global analysis of phenol (PhOH) concentration-dependent TR-PL suggesting that the high energy emitting species is associated with the H-bonded complex, TAHz:PhOH. [PhOH] = 25 mM (red), 50 mM (orange), 75 mM (green), and 100 mM (blue). (A) Kinetic decay rates of slow (solid) and fast (dotted) component with different PhOH concentrations. Slow component decays faster with increasing [PhOH], due to increased Stern-Volmer collisional quenching of unbound TAHz. (B) Normalized SAES reveal that the spectral shape does not appreciably depend on phenol concentration. (C) Intensity of high-energy emission grows with increasing [PhOH] relative to low-energy emission, due to increased H-bonded [TAHz:PhOH] concentration relative to unbound TAHz. Reprinted with permission from Ref. 93. Copyright 2019 American Chemical Society.

Similarly to the time-resolved emission study of TAHz:H₂O that we described above (**Figure 5**), using global target analysis of TR-PL data for TAHz:R-PhOH solutions, we were able to extract wavelength-dependent spectra and time-dependent concentration profiles from distinct emitting species. Data for the specific case of TAHz:PhOH solutions are presented in **Figure 9**. In this case, we observe two different emitting species, one with high-energy SAES and sub-nanosecond decay and the other with low-energy SAES and decay kinetics on the order of a few nanoseconds. These components are labelled “fast” and “slow,” respectively, in **Figure 9B**.⁹³ Interestingly, when the concentration of PhOH was increased from 25 to 100 mM, only the slow component decay was accelerated and the relative intensity of the fast component SAES increased, while the overall spectral shape of both components remained virtually unchanged. This observation strongly supports the assignment of the low-energy emitting, slow component as free TAHz and the high-energy, fast component as the hydrogen bonded TAHz:PhOH complex. When we applied global analysis to other TAHz:R-PhOH samples, we resolved similar two-component emission behavior as well, except for the 4-methoxyphenol case, wherein, the high-energy emission component is absent on the timescale of our measurement. We interpret this result in terms of barrierless reactivity of the

excited TAHz:MeO-PhOH complex, which appears to engage in the PCET reaction prior to emitting measurable fluorescence within the few-picosecond resolution of our streak camera.

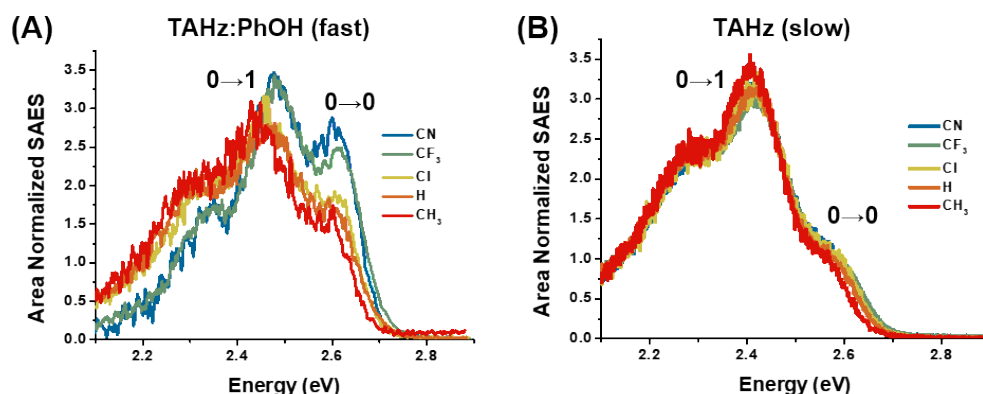


Figure 10 Species-associated emission spectra (SAES) from global analysis of TR-PL from TAHz with R-PhOH solution. A) Significant change in the spectral shape of the fast component depending on the R-group of the phenol: CN (blue), CF₃ (green), Cl (yellow), H (orange), CH₃ (red). B) Slow component spectra show minimal differences among the different R-PhOH. Reprinted with permission from Ref. 120. Copyright 2020 American Chemical Society.

Examining the SAES for the hydrogen bonded TAHz:R-PhOH complexes in our TR-PL data allows us to consider their molecular environments and excited state dynamics in further detail. **Figure 10** shows the fast- and slow-component SAES for various R-PhOH species, ranging from 4-cyanophenol to 4-methylphenol.¹²⁰ Consistent with the assignment of the fast component being associated with the hydrogen bonded complex and the slow component with free TAHz, the SAES line shape of the fast component exhibits significant variation depending on the R-group of the phenolic species. Conversely, the slow SAES components we observe upon introducing TAHz to the range of R-PhOH derivatives are virtually indistinguishable from the free TAHz emission spectrum in toluene. Intriguingly, the variations in spectral shape of the SAES for the H-bonded species appear to exhibit a clear correlation with the electron donating strength of the R group on the phenol. In particular, while the SAES features all appear to exhibit the same vibronic peak spacing, the intensity ratios of the different vibronic peaks, the so-called Franck-Condon progression, change quite dramatically.¹²⁰ In particular, we observe that the highest energy 0-0 vibronic peak becomes more pronounced than the second highest energy or 0-1 peak (**Figure 10A**). This variation of spectral shape is not attributable to variations in the solvent dielectric constant, as we observe virtually

indistinguishable emission spectra for TAHz in toluene vs. a 50:50 mixture of toluene and benzonitrile. Referring to the hydrogen bonding association constants in **Table 1**, we hypothesized that this dramatic distortion of the peak amplitudes, despite no significant variation in the peak spacing, arises as a result of vibronic coupling within the TAHz:R-PhOH complex that influences the extent of the excited state molecular distortion of the TAHz chromophore. As we will describe below, we applied a displaced harmonic oscillator model to capture this trend within the Franck-Condon approximation. We found that stronger hydrogen bonding appears to suppress the nuclear displacement between ground and emitting excited electronic states of TAHz.¹²⁰

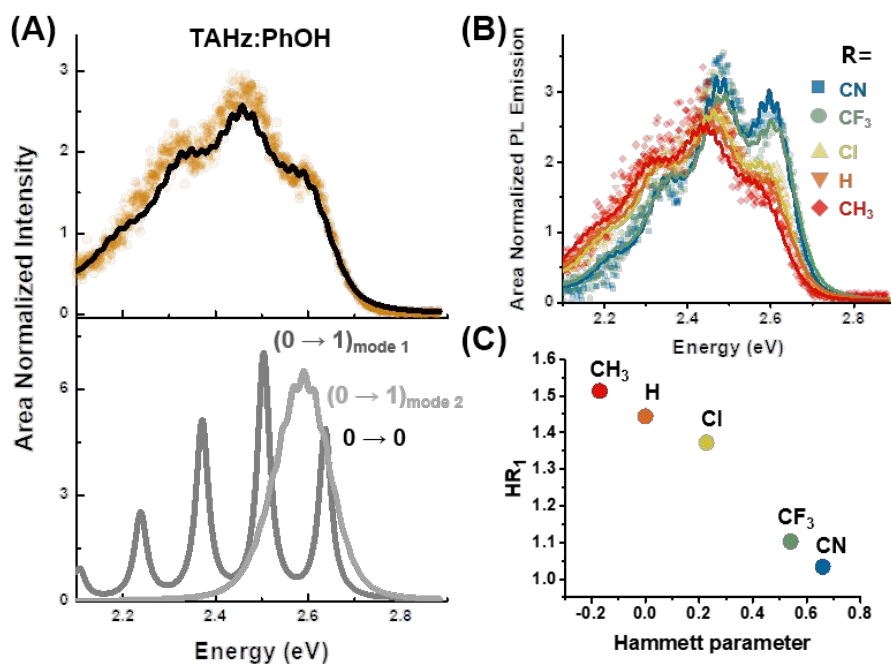


Figure 11 Fitting of fast component emission spectra with displaced harmonic oscillator model of two vibrational modes. A) The extracted TAHz:PhOH emission (orange dots) and fitting with the model (black line), assuming two vibrational modes are coupled to the electronic transition: one high frequency mode around 1050 cm^{-1} , one low frequency mode around 200 cm^{-1} . The bottom plot shows the emission spectra from each of the two vibrational modes independently, with the low frequency mode in light grey and the high frequency mode in dark grey. B) Data (dots) compared to displaced-oscillator model fit (solid lines) for all phenol derivatives. C) The Huang-Rhys parameter for the high frequency mode as a function of Hammett parameter of the para-substituent on phenol. Greater molecular distortion appears to correlate with weaker hydrogen-bonds (lower Hammett parameters). These data suggest that as the intermolecular hydrogen-bonding interaction becomes stronger, the TAHz chromophore in the complex experiences less excited state geometric distortion. Reprinted with permission from Ref. 120. Copyright 2020 American Chemical Society.

Attempts to quantitatively analyze the vibronic structures of TAHz:R-PhOH emission spectra with a single vibrational mode model returned unsatisfactory results. The fast-component SAES cannot be adequately modeled using a single vibrational harmonic oscillator. As in **Figure 11**, at least two vibrational oscillators, a high frequency mode at around 1050 cm^{-1} and a low frequency mode at around 200 cm^{-1} , were required to fit all fast-component SAES from the TAHz:R-PhOH complexes with physically reasonable parameters. We implemented a displaced harmonic oscillator model^{124, 125} where it is assumed that the potential energy surfaces of the electronic ground and excited states comprise the same harmonic potential

and where the equilibrium position of the excited state PES is displaced by d_i along a relevant normal mode coordinate Q_i . The displacement can be quantitatively examined by a dimensionless parameter called the Huang-Rhys parameter,¹²⁶ $HR_i = d_i^2 m_i \omega_i / 2 \hbar$, where m_i is the oscillator effective mass, ω_i is the vibrational frequency of the i^{th} mode, and \hbar is the reduced Planck's constant. Fitting parameters are shown in **Figure 11C** and **Table 2**, along with the electron withdrawing strength of the R-group in the R-PhOH derivatives represented by the Hammett parameter.¹²⁷ As we hypothesized from the spectral shape of the fast component SAES, the HR parameter exhibited a clear trend for both vibrational modes, showing less displacement in the excited state with increasing electron withdrawing character of the R-group. A similar effect showing intra- or inter-molecular hydrogen bonding limiting excited state geometric distortion has been studied in other molecular systems using quantum computational methods.^{128, 129}

R	Hammett Parameter (σ_p)	Mode 1		Mode 2		Calculated H-bond length (Å)
		Frequency (cm^{-1})	HR_1^a	Frequency (cm^{-1})	HR_2	
CH ₃	-0.17	1068.92±0.04	1.513	128.043±0.004	3.6±0.9	1.940
H	0	1070.37±0.05	1.444	185.68±0.02	2.24±0.02	1.937
Cl	0.227	1061.96±0.04	1.372	159.12±0.01	2.36±0.02	1.924
CF ₃	0.54	1057.08±0.05	1.103	179.92±0.04	1.77±0.02	1.910
CN	0.66	1035.49±0.02	1.034	156.800±0.004	1.924±0.007	1.904

^aUncertainty < ±10⁻³

Table 2 Extracted Parameters from fitting with displaced harmonic oscillator model for each vibrational mode.

Reprinted with permission from Ref. 120. Copyright 2020 American Chemical Society.

It is worth noting a few subtleties related to applying the displaced harmonic oscillator analysis to describe the photophysics of the THz chromophore. While our analysis is based on the Franck-Condon and harmonic oscillator approximations, the lowest energy excited state of Hz and THz is a dark $\pi\pi^*$ state, which is technically a symmetry-forbidden electric dipole transition. This is noteworthy since there are several cases of highly symmetric chromophores with symmetry-forbidden excited state transitions, such as pyrene, wherein it has been documented that the radiative transition to ground state cannot be described using only a Franck-Condon type transition, and Herzberg-Teller type transitions¹³⁰ or intensity borrowing effects from higher, bright excited states through solvent dipole – chromophore induced dipole

interactions¹³¹ must be included to satisfactorily describe the emission spectrum. However, based on density functional theory (DFT) calculations, we observe that the hydrogen bonding interaction from R-PhOH to the pyridinic nitrogens of the Hz core breaks the TAHz molecular symmetry, resulting in a significant increase in the oscillator strength of the otherwise dark low-energy $\pi\pi^*$ transition within the electric dipole Franck-Condon approximation.¹²⁰ The oscillator strength induced by this symmetry-breaking effect increases as the R-group of the R-PhOH species becomes more electron withdrawing and the hydrogen bonding interaction in TAHz:R-PhOH becomes stronger. In contrast to the pyrene case, our attempts to model the emission spectra of the TAHz:R-PhOH complexes according to Herzberg-Teller theory could not satisfactorily reproduce the emission line shape when compared with the fits obtained from our displaced oscillator model.

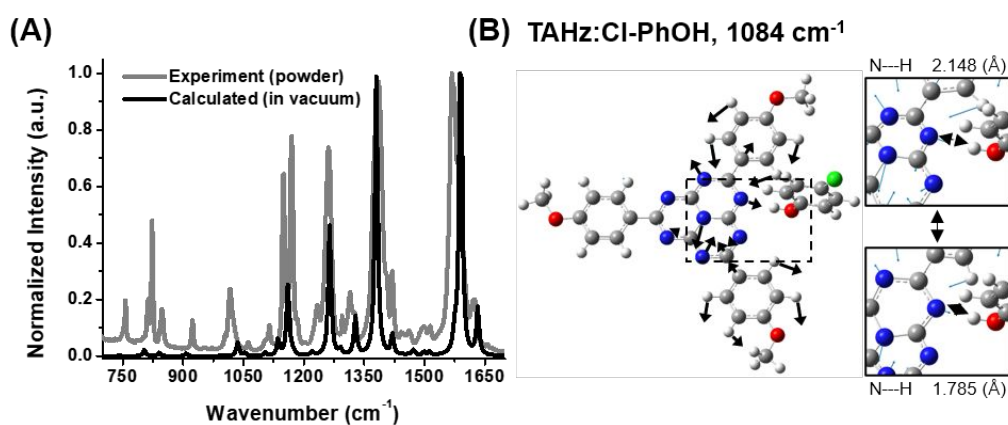


Figure 12 Vibrational mode analysis. (A) FTIR spectrum of TAHz powder (grey) compared to the calculated FTIR spectrum in vacuum (black, frequency is scaled by 0.97). The vibrational modes in the 1000-1200 cm^{-1} region are generally attributable to heptazine ring breathing and C-N stretching modes. (B) An example heptazine ring-breathing vibration of TAHz:Cl-PhOH complex (1084 cm^{-1}) is shown by the displacement vectors. The high frequency mode extracted from the PL spectral fit is attributable to such modes which are able to break symmetry of Hz ring and modulate hydrogen bonding with PhOH. Reprinted with permission from Ref. 120. Copyright 2020 American Chemical Society.

To better visualize the types of vibrational motions associated with the intermolecular vibronic coupling that is evident in the fast component emission spectra we observe in **Figure 10**, we conducted normal mode analyses using DFT calculations. In **Figure 12A** we compare the experimental FT-IR spectrum of TAHz powder with the calculated vibrational spectrum and find that the calculated spectrum agrees adequately

with the experimental data. We next compared vibrational frequencies we obtained from our displaced harmonic oscillator fits (**Table 2**) with the calculated normal modes obtained from DFT for a particular TAHz:R-PhOH complex. Corresponding to the low-frequency mode ($\sim 200\text{ cm}^{-1}$) in the fitting analysis, we found several Hz ring-puckering modes in our calculated spectra in the range $150 - 250\text{ cm}^{-1}$. Therein, the central nitrogen atom in the Hz core is pushed up out of the fused ring plane. This ring-puckering motion is consistent with the optimized geometry of TAHz in the lowest energy dark $\pi\pi^*$ excited state, where the planar symmetry of the Hz ring is broken and the central nitrogen atom pops up in an umbrella-like motion. Since there exist several normal modes with similar ring-puckering motions in our DFT calculations, we conclude that the low-frequency mode and its HR parameter obtained from the displaced oscillator fitting analysis reflect a weighted average of contributing ring-puckering modes.¹³²

In the range $1000 - 1200\text{ cm}^{-1}$, TAHz exhibits a number of normal modes that are generally attributable to Hz ring-breathing motions. One representative ring-breathing mode of the TAHz:Cl-PhOH complex is shown in **Figure 12B**. One relevant feature of the ring-breathing mode is the symmetry breaking effect that it has on the Hz fused ring. Our analysis would suggest that such a displacement of the central and peripheral nitrogen atoms due to this ring-breathing motion may be coupled to the symmetry-breaking effect that supports dipole-allowed emission from the formally dark $\pi\pi^*$ transition. With this vibronic character of ring-breathing motion we assigned ring-breathing modes as the high-frequency mode from fitting analysis in **Table 2**. Another interesting aspect of the ring-breathing motion is that this motion appears to exert a significant modulation of the N-H hydrogen bonding distance. This effect is illustrated in the inset of **Figure 12B**. Evidently, the ring-breathing vibrations affects hydrogen bonding between TAHz and R-PhOH and vice versa. Thus, stronger hydrogen bonding with R-PhOH can hinder geometry distortion in the ring-breathing normal mode coordinate, which ultimately will be reflected in changes of the vibronic structure in the emission spectrum (**Figure 10**). In light of this argument, it is interesting to revisit the different reactivity of 4-chlorophenol vs. phenol in **Table 1**.⁹³ While both cases have nearly identical driving force for electron transfer, the PCET reactivity appears to be more facile for the 4-chlorophenol, which exhibits

stronger hydrogen bonding. From these results, it appears plausible that the PCET reaction is hampered by the geometric distortion of the TAHz excited state, with 4-chlorophenol suppressing this distortion more than phenol, and, hence, showing greater PCET reactivity.

Up to this point, we have considered the effects of chemical modification of the substrate on PCET reactivity. However, considering the nature of the potential energy surfaces along the H atom transfer coordinate, specifically, intermolecular orbital mixing between the chromophore and the substrate may also play a role in facilitating the PCET reaction, as suggested by prior computational results for pyridine,¹³³ triazine,¹³⁴ acridine,¹³⁵ and indeed, more recently, for heptazine.^{85, 88} In particular, for all of these cases mentioned, the hydrogen bonding interactions are not completely innocent, in fact, they play a significant role. That is, the orbitals of the hydrogen bonded complexes comprise hybridized orbital sets with contributions from both the non-bonding orbitals on the heterocycle and *p*-orbital contributions from the oxygen on the hydroxylic species. In the next section we explore this prospect and demonstrate the ability to manipulate the photochemical reactivity of these complexes using multi-pulse excitations that evidentially allow us to access the intermolecular excitations, which appear to be an excited state gateway facilitating the proton-coupled, one electron oxidation of hydroxyl substrates.

III. In-Depth Understanding of Potential Energy Surface and Laser Control of PCET Reaction

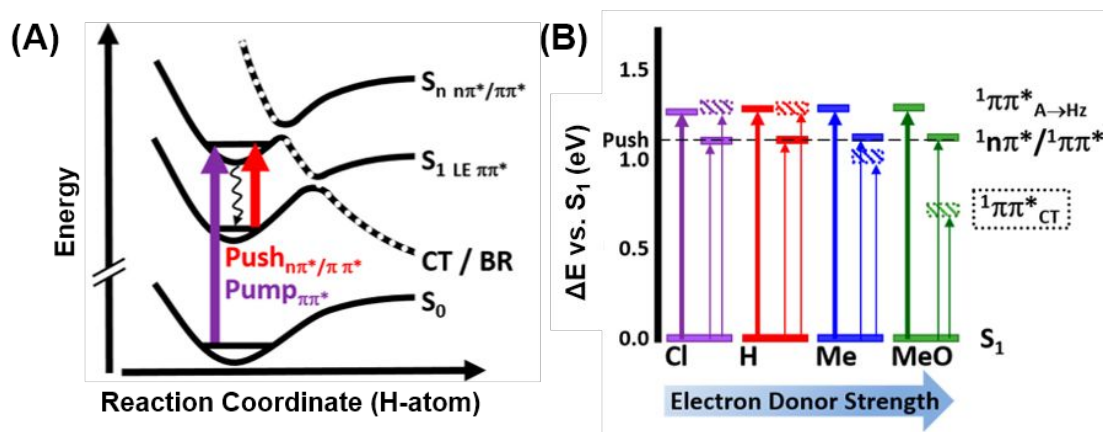


Figure 13 Schematics of multipulse spectroscopy of TAHz:R-PhOH complexes. (A) Potential energy diagram showing a photochemical proton-transfer reaction driven by an electronic charge-transfer (CT) state, which is strongly stabilized by the proton transfer, resulting in the formation of biradical (BR) products. After initial excitation into a bright S_n state, part of the excited population undergoes rapid radiationless decay (black wavy line) into a long-lived S_1 state. The push pulse can then excite this S_1 state population again into a manifold of mixed $n\pi^*/\pi\pi^*$ states that can efficiently couple to the CT state. (B) Simplified energy diagram depicting vertical electronic transition energies from the relaxed geometry of the S_1 state to the $n\pi^*/\pi\pi^*$ states and intermolecular CT state. While the energies of the locally excited states are independent of the substituent R on phenol, the energy of the CT state is substantially lowered by electron-donating substituents such as Me or MeO. Calculated oscillator strengths for transitions are qualitatively represented by the line widths of the vertical arrows. Reprinted with permission from Ref. 117. Copyright 2020 American Chemical Society.

A schematic diagram of the TAHz:R-PhOH potential energy surface is presented in **Figure 13A**. As discussed in above, complexation with various R-PhOH species introduces a new reaction path through an intermolecular CT state along with local excited states of TAHz. Hence in the TAHz:R-PhOH complex, some portion of the initial excited state population traverses the CT state surface, while the remainder of the population will relax into the dark, long-lived $\pi\pi^*$ excited state. The relative energy of the CT state, thus branching ratios among these decay processes, can largely be manipulated by varying the oxidation potential of R-PhOH, as we showed in our previous Stern-Volmer quenching experiments⁹³ and *ab initio* computation results (**Figure 13B**).

Considering the relative energy from the dark $\pi\pi^*$ state to the higher-lying TAHz excited states and the intermolecular CT state, we hypothesized that a secondary excitation pulse could be introduced to

manipulate the photochemical reactivity of the complex. In this case, the second pulse would re-excite some portion of the THz population in the dark $\pi\pi^*$ reservoir state, imparting sufficient additional energy to couple to the CT state, allowing the PCET reaction to proceed more efficiently. The dynamics of the re-excited population could then be probed using a third, broadband probe pulse, in a manner similar to conventional pump-probe transient absorption spectroscopy. Similar multi-pulse approaches, or *pump-push-probe* spectroscopy, have been utilized by a number of research groups to, for example, glean in-depth understanding of the photoexcitation dynamics and photocurrent generation in semiconducting materials.¹³⁶⁻¹³⁸ We employed pump-push-probe spectroscopy for the THz:R-PhOH system in order to evaluate the role that higher excited states play in coupling to the reactive CT state pathway and explore the possibility of optically controlling the trajectory of the PCET reaction.¹¹⁷

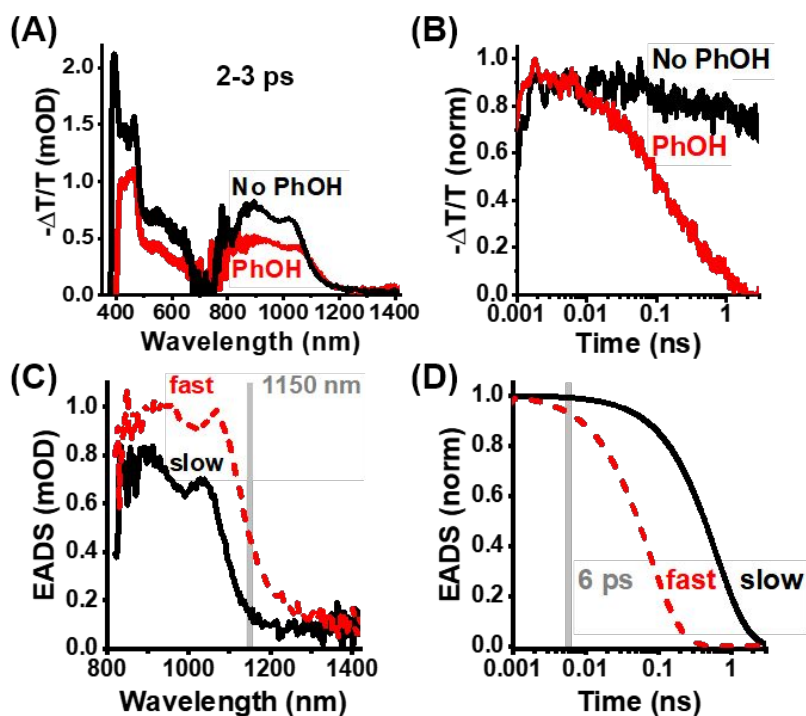


Figure 14 Excited state absorption spectra of the TAHz:PhOH system measured by transient absorption (TA). (A) TA spectra from the ultraviolet to near-infrared (averaged from 2–3 ps) and (B) decay traces of TAHz (15 μM) with and without PhOH (1.0 M) averaged over 900–1000 nm. (C) Spectra and (D) kinetics from global analysis of the NIR transient absorption feature of TAHz in the presence of PhOH. From the evolution-associated difference spectra (EADS), the push pulse was chosen to be 1150 nm to excite the red edge of the lowest-energy transition for the hydrogen-bonded complex (75 ps decay constant, shown in red). The slow component (shown in black) has a decay constant of 620 ps. Reprinted with permission from Ref. 117. Copyright 2020 American Chemical Society.

To monitor excited state absorption spectra of free TAHz and the TAHz:R-PhOH complex in the long-lived dark $\pi\pi^*$ state, we initially performed pump-probe TA spectroscopy with TAHz and TAHz:PhOH mixed samples. **Figure 14A** shows TA spectra of TAHz only and TAHz with PhOH in toluene. The spectra are time-averaged over pump-probe delay times from 2 to 3 ps. After initial excitation into the bright $\pi\pi^*$ state, TAHz undergoes rapid internal conversion to the dark $\pi\pi^*$ S_1 state on a sub-picosecond timescale. The excited TAHz remains in the long-lived S_1 state for several hundred nanoseconds. This is reflected in the experimental TA spectra, showing that after 2 ps the intensity gradually decays and the spectral shape does not change. This assignment is also corroborated by the fact that the decay kinetics of the NIR TA signal (**Figure 14B**) are identical to the time-resolved fluorescence decay of the TAHz S_1 state (not shown

here).¹¹⁷ Based on *ab initio* calculations of the S_1 state (**Figure 13B**), we were able to match the spectral features in the excited state absorption spectra with transitions from the dark $\pi\pi^*$ state. The signal in the NIR region corresponds to the near-degenerate bright $\pi\pi^*$ state and another TAHz excited state with $n\pi^*$ character. There also exists a higher energy $\pi\pi^*$ state transition around 1.8 eV from S_1 which matches with the TA signal around ~690 nm. Consistent with observations from TR-PL experiments, addition of PhOH quenches the S_1 state population via the additional decay and PCET reaction path in the TAHz:PhOH complex and through collisional quenching in the case of free TAHz in the solution, which appears to decrease the signal amplitude (**Figure 14A**) and accelerate the decay kinetics (**Figure 14B**).

Similarly to TR-PL analysis of TAHz:R-PhOH complexes, we can apply global analysis to the TA data for our TAHz:PhOH samples to recover detailed kinetic information. The data can be modeled with two excited species, one with a fast, ~75 ps decay constant, and the other with a slow, 620 ps decay constant. We attributed the fast component to the TAHz:PhOH complex and the slow component to free TAHz, following our previous analysis of the TR-PL decay kinetics. We selected a pulse wavelength of 1150 nm for the secondary excitation in the pump-push-probe experiment in order to exclusively ‘push’ only the TAHz:PhOH complex in the S_1 state to the mixed $n\pi^*/\pi\pi^*$ state. This selection was based upon evolution-associated decay spectra (EADS) of each component in **Figure 14C**. The 6 ps delay between pump and push pulse was chosen to ensure that complete internal conversion to the S_1 state occurred after the initial excitation and that the push pulse has a chance to interact with the S_1 population before it completely decays.

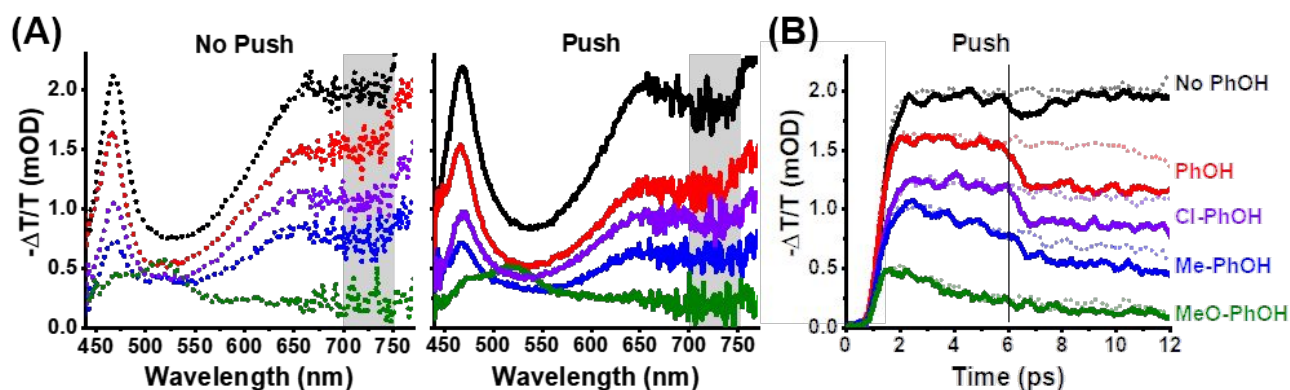


Figure 15 Effect of push pulse from pump-push-probe spectroscopy. (A) (Left, dotted) Pump-probe spectra of TAHz (50 μ M) in toluene with and without phenol derivatives, R-PhOH (1 M). (Right, solid) Pump-push-probe spectra of TAHz (50 μ M) in toluene with and without phenol derivatives, R-PhOH (1 M). Spectra were averaged from 6.5–8.0 ps. (B) Decay of the S_1 state population probed from 700–750 nm, shaded in gray in (A), with (solid) and without (dotted) the push pulse. The system was pumped at 365 nm and pushed at 1150 nm at 6 ps. The sample was continuously stirring during the experiment. Reprinted with permission from Ref. 117. Copyright 2020 American Chemical Society.

Figure 15A shows visible to NIR region TA spectra from toluene solutions of TAHz and a TAHz:R-PhOH, with and without the 1150 nm push pulse (6 ps delay with respect to the 365 nm pump excitation). There are two notable aspects in the data. First, we identified the same general reactivity trend that we observed in our TR-PL data. The R-PhOH species possessing R-groups with greater electron donating character tend to quench more of the excited state TAHz population. Experimentally, this result manifests as decreased signal amplitude in TA spectra among these samples at equivalent pump-probe delays. Interestingly, the spectral shape of the TA signal was completely different, with a peak around 520 nm, in the case of 4-methoxyphenol, where the PCET reaction becomes barrierless. The latter being consistent with TR-PL measurements and quantum chemical calculations. We hypothesized that the excited TAHz:MeO-PhOH complex primarily couples to the CT state and results in biradical products. This may be the origin of the distinct TA spectrum in the MeO-PhOH case, perhaps comprising the TAHz-H $^{\bullet}$ radical absorption. Secondly, the effect of the push pulse appears in the TA spectra, with varying degrees depending on the substrate, as a decrease in the S_1 state population that is concomitant with the arrival of the push pulse. The depletion of S_1 state population is most clearly discernible in time-resolved decay kinetics in **Figure 15B**. We observed that the depopulation of the S_1 state absorption for the TAHz:PhOH case persists following the arrival of the push pulse, which means that the depletion of S_1 state population is irreversible.

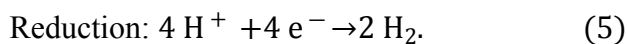
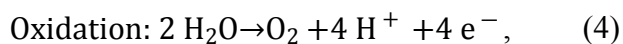
In other words, the push pulse drives the S_1 population along an alternate chemical trajectory, likely via the CT state pathway along the PCET reaction coordinate, rather than returning to the dark $\pi\pi^*$ state. This result is in sharp contrast to the behavior of the S_1 state in response to the arrival of the push pulse in the THz only case, where the CT state is absent. In the THz-only case, the re-excited population can only relax back to the S_1 state. Thus, there is only a transient depopulation of the S_1 state and the TA signal exhibits a rapid recovery, approaching the response resolution of our pump-push-probe instrumentation for the THz only case.

The results from pump-push-probe experiments are congruous with the molecular picture from our TR-PL experiments and computational analysis, as schematically summarized in **Figure 7**. Hydrogen bonding with R-PhOH introduces an intermolecular CT state to the THz potential energy surface, along which a portion of the photoexcited population in the bright S_n state can traverse to undergo PCET, resulting in biradical products. On the other hand, the portion of the population that rapidly relaxes into the long-lived S_1 state undergoes a molecular distortion, which opens a pathway for these excitations to be re-excited by the push pulse to a mixed $n\pi^*/\pi\pi^*$ state that can effectively couple to the reactive CT pathway. The relative energy of the CT state compared to other THz excited states can be modulated by chemically modifying the R-PhOH oxidation potential, and consequently the branching ratio between PCET path and relaxation to S_1 can be manipulated. In the limit of 4-methoxyphenol, a barrierless PCET reaction condition is achievable and the vast majority of the photoexcited population traverses the reactive CT coordinate. The relative effect of the push pulse, the persistent bleaching of S_1 state absorption signal intensity (**Figure 15**), appears to mirror this reactivity trend. The less reactive R-PhOH (phenol) species exhibit large activation barriers and less efficient coupling to the CT state. In this case, due to the higher potential energy barrier, more of the photoexcited population relaxes into the S_1 manifold rather than proceeding into the CT state. The push pulse re-excites a greater fraction of the remaining unreacted THz S_1 states to the higher-lying mixed $n\pi^*/\pi\pi^*$ state with phenol than other R-PhOHs. Thus, the fractional push pulse effect that we observe is more pronounced with PhOH than for the other R-PhOH complexes. In the case of 4-

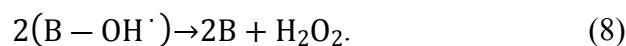
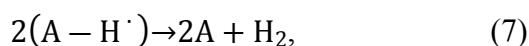
methoxyphenol, the photoexcited THz primarily engages in the PCET reaction, with little remaining population relaxing to the S_1 state that could be re-excited by the push pulse. Consequently, we observe a vanishingly small effect of the push pulse in the MeO-PhOH case.

Future Directions for Photoactive Heptazines

If one considers the water splitting reaction, the most conceptually simple set of half reactions involves a pair of four-electron and four-proton redox processes, as shown below:¹⁷



Energetically, this water splitting process to generate oxygen and hydrogen must be driven with an external energy source, typically provided by electrical input or a combination of photon energy and electrochemical impulse. To support photon-driven water splitting, sensitizers for absorbing incident light and catalysts for facilitating electron transfer have been explored.^{13, 17} However, it has been widely recognized that multi-electron redox reactions, especially the four-electron oxidation reaction (**Eq. 4**), are kinetically unwieldy and this limitation hampers efficient water splitting with diffuse solar illumination.¹³⁹ Historically, pathways for water oxidation involving intermediates with radical character have been deliberately avoided, due to the perception that they are inherently untamable energy loss processes.¹⁴⁰ However, that notion presupposes such neutral open-shell species to necessarily be H^\cdot or $\cdot\text{OH}$ free radicals. In fact, the reducing and oxidizing equivalents generated following a photon-driven cleavage of an intermolecular hydrogen bonded complex by PCET can be stabilized by the surrounding complexation environment. As such, one may conceive of pathways alternative to standard proton reduction for hydrogen generation:^{84, 100}



In this case, A is the photoactive catalyst that is capable of hydrogen bonding and excited state PCET and B is a co-catalyst for stabilizing $\cdot\text{OH}$ radicals, such as noble metals or metal oxides.^{100, 141, 142} This scenario avoids kinetically cumbersome multi-electron redox processes and may be amendable to utilizing low-intensity light sources, including solar irradiation. In this regard, the Hz molecular catalyst may satisfy two important preconditions for acting as a photoactive catalyst for water splitting: 1) Hz can form hydrogen

bonded complexes through its peripheral nitrogen atoms and 2) undergo intermolecular PCET reactions that result in biradical products. In the preceding sections of this Feature Article, we have discussed at length the computational and experimental evidence for these two qualities that our previous research has provided.

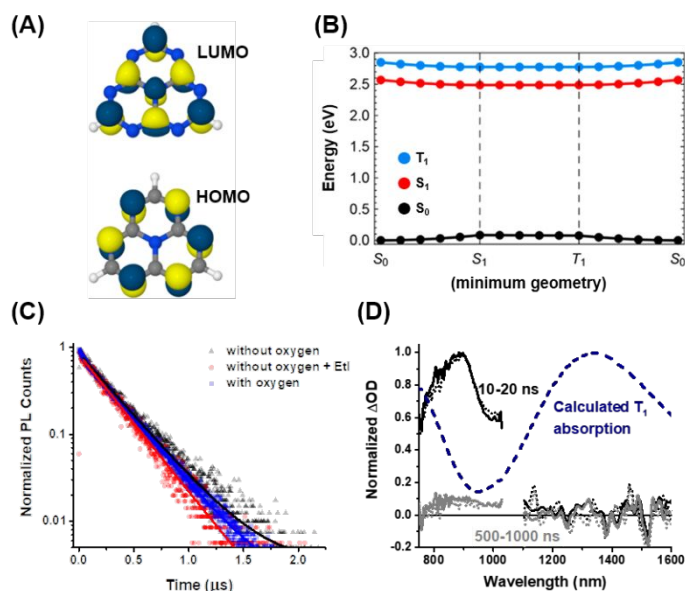


Figure 16 Relevant molecular orbitals and inverted S_1/T_1 energy of Hz derivatives. (A) Highest occupied (HOMO) and lowest unoccupied (LUMO) Hartree–Fock molecular orbitals of Hz, which constitute the major transition character of the S_1 excited state. (B) Energy profiles of linearly interpolated scans between the S_0 minimum geometry, the S_1 minimum geometry, and the T_1 minimum geometry of Hz, calculated at the ADC(2) level. The energy of the T_1 state (blue) is above the energy of the S_1 state (red) throughout. Black trace corresponds to the energy of the S_0 state at each geometry. (C) Emission lifetimes of TAHZ in toluene show very little dependence on the presence of oxygen or a heavy atom source, such as ethyl iodide (EtI). Comparing the emission decay with (blue) and without oxygen (black), and at various temperatures, we see no evidence for a low energy triplet quenching pathway or thermally activated delayed fluorescence. (D) TA spectra with (dotted) and without (solid) the presence of a heavy atom at early (black) and long (gray) timescales. Data show no significant difference. For comparison, calculated triplet state absorption (dashed line) is also presented. Reprinted with permission from Ref. 143. Copyright 2019 American Chemical Society.

One important remaining factor that influences the photochemical reactivity of Hz derivatives may, at first glance, appear to be a rather subtle detail associated with their electronic structures. However, upon further examination, this feature results in important and quite unique behavior. **Figure 16A** shows the Hz molecular orbitals associated with the dark $\pi\pi^*$ S_1 state, calculated at the ADC(2) level of theory. The HOMO is entirely localized on the peripheral nitrogen atoms, while the LUMO is localized on the carbon atoms. Nearly zero overlap exists among the two MOs,¹⁴³ despite their localization on the Hz core of the

molecule. The near-zero overlap results in an electron exchange energy that is uncharacteristically small for most organic molecules, such that the singlet and triplet excited states would be, to first order, nearly degenerate. However, due to spin-polarization effects,^{144, 145} the energy ordering of the S_1 and T_1 states actually becomes inverted with respect to what one would normally anticipate from Hund's multiplicity rules. As a result, the T_1 state is higher in energy than the stabilized S_1 state in Hz derivatives. Since observing this stabilization computationally requires coupling with double excitations,¹⁴⁴ the correct energy ordering for these states cannot be recovered using DFT methods, whereas it is readily observed in the ADC(2) calculations for several Hz derivatives (**Figure 16B**). Moreover, we applied a number of spectroscopic methods to assess the qualitative energy ordering of these different spin states. TR-PL experiments conducted for TAHz under aerobic vs. anaerobic conditions, as well as in the presence of an external heavy atom sensitizer (**Figure 16C**) all indicated the absence of a viable low-energy triplet pathway by which the S_1 state can be quenched.¹⁴³ We obtained analogous results using transient absorption spectroscopy (**Figure 16D**). The unique nature of the intersystem crossing to T_1 from S_1 being energetically uphill in Hz derivatives, means that deactivation of the photoexcited S_1 state has only two primary deactivation pathways, photon emission or internal conversion to S_0 . We stressed earlier that the dark $\pi\pi^*$ transition in Hz and its derivatives is symmetry-forbidden, however, since the energy gap between the S_1 and the S_0 state is relatively large, the rate constant for internal conversion between these states is small, in accord with Energy Gap Law.¹⁴⁶ Therefore, despite the weak oscillator strength for the S_1 transition, which leads to a particularly long fluorescence lifetime (287 ns), the fluorescence quantum yield is unexpectedly high (~70% in toluene).¹¹³ This combination of unusual attributes allows the S_1 excitations to act as long-lived reservoir states for photochemical reactions, while avoiding generating long-lived triplet excitations that would be susceptible to sensitizing reactive singlet oxygen that can destroy the catalyst. The latter is a common drawback associated with photocatalysts that rely on generating triplet excited states with lifetimes long enough to outlast the slow timescales for molecular diffusion.

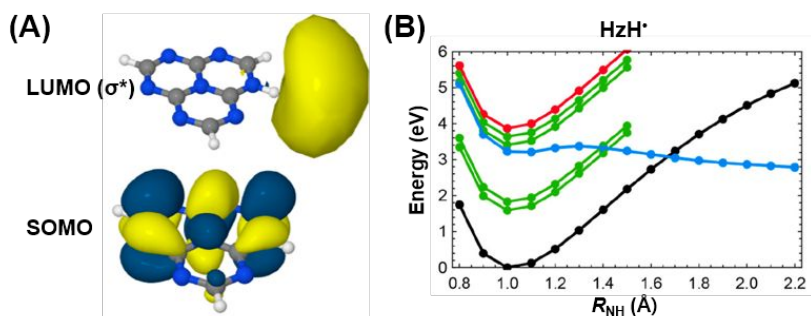


Figure 17 Heptazinyl radical photodissociation. (A) Singly occupied molecular orbital (SOMO) and the unoccupied diffusive σ^* orbital involved in the excitation of the ${}^2\Pi\sigma^*$ state of the HzH• radical. (B) Potential energy surface of HzH• radical along N-H distance. Black = ground state, green = $\Pi\Pi^*$ excited states, red = $n\Pi^*$ excited states, blue = repulsive $\Pi\sigma^*$ state. The repulsive $\Pi\sigma^*$ state provides a photodissociation channel for H atom detachment reaction. Reprinted with permission from Ref. 147. Copyright 2020 American Chemical Society.

Apart from the PCET reactivity and biradical formation, it is also worth considering the subsequent reactivity of the heptazinyl radical (HzH•) and its potential photochemistry following the initial H atom abstraction.¹⁴⁷ **Figure 17** illustrates a computational survey of the excited states of HzH•. Notably, one of the electronic excited states of the heptazinyl radical exhibits dissociative character along the Hz-H• bond axis. Excitation of HzH• into this dissociative $\pi\sigma^*$ state, where the electron occupies a Rydberg-type orbital, will result in H• radical emission. This process would restore the closed-shell ground state neutral Hz chromophore, which can then ultimately reengage in subsequent PCET reactions with additional substrate molecules. In this scenario, light energy will be converted into reactive H• and substrate radical, which can be used to facilitate subsequent reactions, while the Hz catalyst is regenerated, avoiding persistent chemical decomposition. Based on this result, photocatalysis and catalyst regeneration are viable through a multi-pulse excitation scheme, without degradation from side reactions. The multi-pulse experiments are currently ongoing in order to spectroscopically probe biradical products and also photoexcite the product into the dissociative electronic state, exploring another possibility of manipulation of heptazine photochemistry.

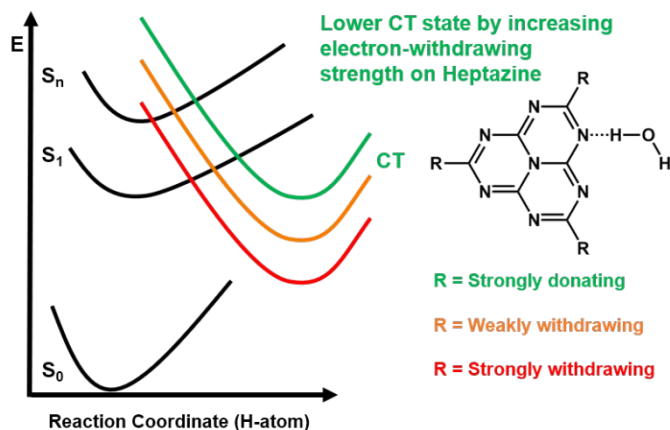


Figure 18 Schematic diagram of potential energy surfaces for substituted Hz:H₂O complexes, illustrating the relationship between the relative energy of the CT state and the PCET barrier on the PE surface of the S₁ state. Reprinted with permission from Ref. 147. Copyright 2020 American Chemical Society.

Experimental and computational evidence suggests that one major factor determining PCET reactivity between the TAHz catalyst and the R-PhOH substrate is the nature of the barrier between the non-reactive TAHz electronic states and the reactive intermolecular CT states of the complex.⁹³ We were able to tune the reactivity in our previous studies by changing the R-group of the R-PhOH substrate, due simply to a change in oxidation potential. Considering the fact that the relative energy is important in determining PCET reactivity, one can envisage that a reciprocal strategy could be employed by incorporating electron withdrawing pendant groups on the Hz core to tune the CT state energy barrier and increase PCET reactivity (**Figure 18**).¹⁴⁷ One of the most important substrates in photocatalysis, the water molecule, cannot be modified as R-PhOH, and thus we can modify Hz catalysts itself to optimize reactivity for more efficient water oxidation chemistry. Synthetic approaches in this respect are currently ongoing in our lab. We also continue to explore multi-pulse excitation schemes to better understand photochemistry of heptazine derivatives in greater detail and develop more effective molecular photocatalyst systems.

Summary

In this Feature Article, we presented our recent research efforts regarding the photochemistry of polymeric g-C₃N₄ and derivatives of its structural monomer unit, heptazine (Hz). From our initial time-resolved spectroscopic analysis on g-C₃N₄ and exfoliated C₃N₄ flakes¹⁰² we speculated that the primary reactive sites where photocatalysis occurs may be molecular Hz sub-units of g-C₃N₄.¹¹⁰ Computational analysis of Hz derivatives and other N-heterocyclic molecules suggest that hydrogen bond formation and subsequent PCET reactions may influence g-C₃N₄ photocatalysis, leading to prospects for thermodynamic and kinetic advantages.⁸⁸ Consistent with this prediction, we experimentally observed that our model Hz derivative, TAHz, can form hydrogen bonded complexes with water, undergo photon-driven PCET, and generate [•]OH and H₂ products.¹¹³ Using R-PhOH substrates, we were able to uncover additional quantitative assessments of hydrogen bonding strength and PCET reactivity related to spectroscopically-determined association constants and Stern-Volmer quenching rate constants.⁹³ The results followed a general trend that the oxidation potential of the R-PhOH species is a primary factor governing the activity, such that a substrate with lower oxidation potential is more likely to transfer its electron to TAHz. That is, couple to the intermolecular CT state and progress along the PCET reaction pathway. *Ab initio* calculations successfully reproduced the same trend as the experimental results. The barrierless PCET condition is experimentally achievable using the 4-methoxyphenol substrate. Additionally, we were able to analyze aspects of the molecular environment and its influence on the properties of excited-state TAHz:R-PHOH complexes through a vibronic analysis of their time-resolved emission spectra. Fitting the TR-PL data from the hydrogen bonded complex with a multi-mode displaced harmonic oscillator model and comparing the result with DFT calculation,¹²⁰ indicates that increasing the electron withdrawing character of the R-group (higher Hammett parameter) induces stronger hydrogen bonding between TAHz and R-PhOH. This H-bonding effect evidently suppresses the geometric distortion between the S₁ state and the S₀ ground state. Consequently, we observe a lower Huang-Rhys parameter in the measured fluorescence spectra with increasing Hammett parameter. Manipulating the hydrogen bonding strength may provide an additional

control knob for tuning PCET reactivity, which is evidently at play in cases of similar redox potentials of the Hz derivative or the substrate, such as in the instance of TAHz:PhOH vs. TAHz:Cl-PhOH. Lastly, we explored another possible way to control the TAHz photoreaction: optical control with multi-pulse spectroscopy.¹¹⁷ When we introduced a NIR secondary excitation pulse (the push pulse in **Figure 13**) that can excite TAHz in the S_1 state into higher excited states, we observed a persistent depletion of the S_1 state population of the TAHz:PhOH complex. This is in contrast to the free TAHz case, wherein the depletion is only transient. The amount of depletion also followed the trend in the PCET reactivity of the R-PhOH species, which is consistent with the molecular picture from our previous TR-PL studies. That is, a greater fraction of the initially excited population proceeds along the PCET pathway as the R-PhOH species becomes easier to oxidize. Thus, fewer of the excited complexes relax into the S_1 state to be re-excited by the push pulse. Since the push-induced depletions of the population does relax back to the S_1 state, the implication is that this re-excited population has coupled into the reactive intermolecular CT state as a result of the additional energy imparted by the push pulse.

In this Feature Article, we focus primarily on light-driven water oxidation reactions of Hz-based materials. However, it is also a critical challenge to understand analogous molecular mechanisms involved in other important chemical transformations, such as CO_2 reduction, which has been reviewed extensively in the literature.¹⁴⁸⁻¹⁵⁰ For example, recently, Domcke, Sobolewski and coworkers predicted that pyridinyl radicals are capable of hydrogen-bonding with and chemically reducing CO_2 by photoinduced PCET.¹⁵¹ The authors noted that a similar mechanism may provide insight into the photocatalytic reduction of CO_2 by g- C_3N_4 . The implication being that photogenerated heptazinyl radicals (HzH \cdot) can form hydrogen-bonded complexes with CO_2 . The complexes can then photodissociate by a PCET process to liberate hydroxyformyl radicals. Recent experimental studies indicate that employing co-polymerization¹⁵² or introducing structural defects¹⁵³⁻¹⁵⁵ to C_3N_4 can increase activity toward CO_2 reduction. Our work suggests that experimental approaches utilizing model molecular Hz derivatives may provide additional insight into the CO_2 reduction mechanisms for C_3N_4 . Hydroamidation reactions are another notable class of

transformations that have recently been affected using C_3N_4 -based photocatalysts. In a recent example from Nocera and coworkers, the authors demonstrated that cyanamide-modified C_3N_4 can initiate a light-driven PCET process that catalyzes a hydroamidation photoredox cycle involving a number of H-atom transfer steps.⁵⁵

While this Feature Article has primarily dealt with optical spectroscopic techniques such as time-resolved photoluminescence and transient absorption spectroscopy, other time-resolved methods may provide additional insight into the photoreactivity mechanisms of C_3N_4 and heptazine-based materials. For example, a recent two-dimensional IR analysis revealed the picosecond intramolecular vibrational energy redistribution process in g- C_3N_4 .¹⁵⁶ Time-resolved microwave conductivity¹⁵⁷ and optical-pump terahertz-probe spectroscopy¹⁵⁸ have also been used to directly measure photoconductivity of C_3N_4 -based catalysts, correlating conductivity with catalytic efficiency.

Finally, the inverted S_1/T_1 energy splittings (ΔE_{ST}) that Hz derivatives exhibit remain one of their truly remarkable attributes. Arising from the combination of higher-order spin polarization effects and their localized, but non-overlapping HOMO and LUMO character, this ΔE_{ST} inversion, paired with the forbidden nature of the S_1 fluorescence, leads to an uncharacteristically high fluorescence quantum efficiency ($\sim 70\%$) for a material with such a long fluorescence lifetime (~ 300 ns).¹⁴³ These photophysical properties are important for photochemical applications because they allow the S_1 state to serve as a long-lived energy reservoir, supporting molecular diffusion, while avoiding the sensitization of indiscriminately-reactive singlet oxygen. The latter often induces uncontrollable catalyst degradation and plagues many long-lived triplet photocatalytic systems.

It also seems likely that Hz-based materials will serve as a model testbed for better understanding and applying inverted ΔE_{ST} motifs in the field of thin-film optoelectronic materials and devices that incorporate organic semiconductor components. This will undoubtedly be particularly true for organic LEDs and organic photovoltaics, where device performance is often sensitive to recombination processes involving triplet excitons. The same may perhaps be true even for perovskite-based devices that incorporate organic

charge transport layers. All told, Hz-based materials appear poised to be of increasing relevance for numerous potential applications, ranging from photocatalysis for sustainable energy technologies and preparatory photochemistry to solid-state optoelectronic materials and devices.

AUTHOR INFORMATION

Corresponding Author

*Cody W. Schlenker, Email: schlenk@uw.edu

Author Contributions

The manuscript was written through contributions of all authors. All authors have given approval to the final version of the manuscript.

ORCID

Doyk Hwang: 0000-0001-5275-0354

Cody W. Schlenker: 0000-0003-3103-402X

Notes

The authors declare that there are no competing financial interests.

ACKNOWLEDGMENTS

This work is based on research that was supported in part by the Washington Research Foundation and the University of Washington Clean Energy Institute (CEI). Part of this work was conducted at the Molecular Analysis Facility, a National Nanotechnology Coordinated Infrastructure (NNCI) site at the University of Washington, which is supported in part by funds from the National Science Foundation (awards NNCI-2025489, NNCI-1542101), the Molecular Engineering & Sciences Institute, and the Clean Energy Institute. DFT and TD-DFT calculations were facilitated through the use of advanced computational, storage, and networking infrastructure provided by the Hyak supercomputer system and funded by the STF at the

University of Washington. C. W. S. acknowledges that a portion of this material is based upon work supported by the US National Science Foundation (NSF) under Grant No. [1846480]. We would also like to express our appreciation to Prof. Dr. habil. Wolfgang Domcke and Prof. Dr. hab. Andrzej L. Sobolewski for their invaluable *ab initio* computational contributions to many of the works discussed in this article.

REFERENCES

1. Lewis, N. S., Research opportunities to advance solar energy utilization. *Science* **2016**, *351* (6271), aad1920.
2. Qu, Y.; Duan, X., Progress, challenge and perspective of heterogeneous photocatalysts. *Chem Soc Rev* **2013**, *42* (7), 2568-80.
3. Battaglia, C.; Cuevas, A.; De Wolf, S., High-efficiency crystalline silicon solar cells: status and perspectives. *Energy & Environmental Science* **2016**, *9* (5), 1552-1576.
4. Gong, J.; Li, C.; Wasielewski, M. R., Advances in solar energy conversion. *Chem Soc Rev* **2019**, *48* (7), 1862-1864.
5. Shaw, M. H.; Twilton, J.; MacMillan, D. W., Photoredox Catalysis in Organic Chemistry. *J Org Chem* **2016**, *81* (16), 6898-926.
6. Gentry, E. C.; Knowles, R. R., Synthetic Applications of Proton-Coupled Electron Transfer. *Acc Chem Res* **2016**, *49* (8), 1546-56.
7. Savateev, A.; Antonietti, M., Heterogeneous organocatalysis for photoredox chemistry. *ACS Catalysis* **2018**, *8* (10), 9790-9808.
8. Protti, S.; Fagnoni, M.; Ravelli, D., Photocatalytic C-H Activation by Hydrogen-Atom Transfer in Synthesis. *ChemCatChem* **2015**, *7* (10), 1516-1523.
9. Colmenares, J. C.; Luque, R., Heterogeneous photocatalytic nanomaterials: prospects and challenges in selective transformations of biomass-derived compounds. *Chem Soc Rev* **2014**, *43* (3), 765-78.
10. Rugolo, J.; Aziz, M. J., Electricity storage for intermittent renewable sources. *Energy & Environmental Science* **2012**, *5* (5), 7151-7160.
11. Shaner, M. R.; Davis, S. J.; Lewis, N. S.; Caldeira, K., Geophysical constraints on the reliability of solar and wind power in the United States. *Energy & Environmental Science* **2018**, *11* (4), 914-925.
12. Pinaud, B. A.; Benck, J. D.; Seitz, L. C.; Forman, A. J.; Chen, Z.; Deutsch, T. G.; James, B. D.; Baum, K. N.; Baum, G. N.; Ardo, S., Technical and economic feasibility of centralized facilities for solar hydrogen production via photocatalysis and photoelectrochemistry. *Energy & Environmental Science* **2013**, *6* (7), 1983-2002.

13. Maeda, K.; Domen, K., Photocatalytic water splitting: recent progress and future challenges. *The Journal of Physical Chemistry Letters* **2010**, *1* (18), 2655-2661.
14. Takanabe, K., Photocatalytic water splitting: quantitative approaches toward photocatalyst by design. *ACS Catalysis* **2017**, *7*(11), 8006-8022.
15. Walter, M. G.; Warren, E. L.; McKone, J. R.; Boettcher, S. W.; Mi, Q.; Santori, E. A.; Lewis, N. S., Solar water splitting cells. *Chem Rev* **2010**, *110*(11), 6446-73.
16. Li, J.; Güttinger, R.; Moré, R.; Song, F.; Wan, W.; Patzke, G. R., Frontiers of water oxidation: the quest for true catalysts. *Chem Soc Rev* **2017**, *46* (20), 6124-6147.
17. Blakemore, J. D.; Crabtree, R. H.; Brudvig, G. W., Molecular Catalysts for Water Oxidation. *Chem Rev* **2015**, *115* (23), 12974-3005.
18. Karkas, M. D., Photochemical generation of nitrogen-centered amidyl, hydrazonyl, and imidyl radicals: methodology developments and catalytic applications. *ACS Catalysis* **2017**, *7*(8), 4999-5022.
19. Gaya, U. I.; Abdullah, A. H., Heterogeneous photocatalytic degradation of organic contaminants over titanium dioxide: a review of fundamentals, progress and problems. *Journal of photochemistry and photobiology C: Photochemistry reviews* **2008**, *9*(1), 1-12.
20. Wang, C.-C.; Li, J.-R.; Lv, X.-L.; Zhang, Y.-Q.; Guo, G., Photocatalytic organic pollutants degradation in metal-organic frameworks. *Energy & Environmental Science* **2014**, *7*(9), 2831-2867.
21. Hammes-Schiffer, S., Controlling Electrons and Protons through Theory: Molecular Electrocatalysts to Nanoparticles. *Acc Chem Res* **2018**, *51* (9), 1975-1983.
22. Gagliardi, C. J.; Vannucci, A. K.; Concepcion, J. J.; Chen, Z.; Meyer, T. J., The role of proton coupled electron transfer in water oxidation. *Energy & Environmental Science* **2012**, *5* (7), 7704-7717.
23. Bourrez, M.; Steinmetz, R.; Ott, S.; Gloaguen, F.; Hammarström, L., Concerted proton-coupled electron transfer from a metal-hydride complex. *Nat Chem* **2014**, *7*(2), 140-5.
24. Liu, T.; Guo, M.; Orthaber, A.; Lomoth, R.; Lundberg, M.; Ott, S.; Hammarström, L., Accelerating proton-coupled electron transfer of metal hydrides in catalyst model reactions. *Nat Chem* **2018**, *10*(8), 881-887.
25. Tyburski, R.; Liu, T.; Glover, S. D.; Hammarström, L., Proton-Coupled Electron Transfer Guidelines, Fair and Square. *J Am Chem Soc* **2021**, *143* (2), 560-576.
26. Kamat, P. V.; Christians, J. A., Solar Cells versus Solar Fuels: Two Different Outcomes. *J Phys Chem Lett* **2015**, *6*(10), 1917-8.
27. Chu, S.; Li, W.; Yan, Y.; Hamann, T.; Shih, I.; Wang, D.; Mi, Z., Roadmap on solar water splitting: current status and future prospects. *Nano Futures* **2017**, *1* (2), 022001.

28. Hu, S.; Xiang, C.; Haussener, S.; Berger, A. D.; Lewis, N. S., An analysis of the optimal band gaps of light absorbers in integrated tandem photoelectrochemical water-splitting systems. *Energy & Environmental Science* **2013**, *6* (10), 2984-2993.
29. Jia, J.; Seitz, L. C.; Benck, J. D.; Huo, Y.; Chen, Y.; Ng, J. W.; Bilir, T.; Harris, J. S.; Jaramillo, T. F., Solar water splitting by photovoltaic-electrolysis with a solar-to-hydrogen efficiency over 30. *Nat Commun* **2016**, *7*, 13237.
30. Cheng, W.-H.; Richter, M. H.; May, M. M.; Ohlmann, J.; Lackner, D.; Dimroth, F.; Hannappel, T.; Atwater, H. A.; Lewerenz, H.-J., Monolithic photoelectrochemical device for direct water splitting with 19% efficiency. *ACS Energy Letters* **2018**, *3* (8), 1795-1800.
31. Shaner, M. R.; Atwater, H. A.; Lewis, N. S.; McFarland, E. W., A comparative technoeconomic analysis of renewable hydrogen production using solar energy. *Energy & Environmental Science* **2016**, *9* (7), 2354-2371.
32. James, B. D.; Baum, G. N.; Perez, J.; Baum, K. N., Technoeconomic analysis of photoelectrochemical (PEC) hydrogen production. *DOE report* **2009**.
33. Kudo, A.; Miseki, Y., Heterogeneous photocatalyst materials for water splitting. *Chem Soc Rev* **2009**, *38* (1), 253-78.
34. Wang, Q.; Domen, K., Particulate Photocatalysts for Light-Driven Water Splitting: Mechanisms, Challenges, and Design Strategies. *Chem Rev* **2020**, *120* (2), 919-985.
35. Xu, Y.; Kraft, M.; Xu, R., Metal-free carbonaceous electrocatalysts and photocatalysts for water splitting. *Chem Soc Rev* **2016**, *45* (11), 3039-52.
36. Rahman, M. Z.; Kibria, M. G.; Mullins, C. B., Metal-free photocatalysts for hydrogen evolution. *Chem Soc Rev* **2020**, *49* (6), 1887-1931.
37. Li, L.; Lo, W.-y.; Cai, Z.; Zhang, N.; Yu, L., Donor-acceptor porous conjugated polymers for photocatalytic hydrogen production: the importance of acceptor comonomer. *Macromolecules* **2016**, *49* (18), 6903-6909.
38. Chen, H. Y.; Ardo, S., Direct observation of sequential oxidations of a titania-bound molecular proxy catalyst generated through illumination of molecular sensitizers. *Nat Chem* **2018**, *10* (1), 17-23.
39. Bredas, J. L.; Street, G. B., Polarons, bipolarons, and solitons in conducting polymers. *Accounts of Chemical Research* **1985**, *18* (10), 309-315.
40. Caspar, J. V.; Ramamurthy, V.; Corbin, D. R., Preparation and spectroscopic characterization of polarons and bipolarons of thiophene oligomers within the channels of pentasil zeolites: the evolution of organic radical ions into conducting polymers. *Journal of the American Chemical Society* **1991**, *113* (2), 600-610.

41. Zheng, S.; Barlow, S.; Risko, C.; Kinnibrugh, T. L.; Khrustalev, V. N.; Jones, S. C.; Antipin, M. Y.; Tucker, N. M.; Timofeeva, T. V.; Coropceanu, V., Isolation and crystal structures of two singlet bis (triarylamine) dications with nonquinoidal geometries. *Journal of the American Chemical Society* **2006**, *128* (6), 1812-1817.
42. Dhanker, R.; Gray, C. L.; Mukhopadhyay, S.; Nunez, S.; Cheng, C. Y.; Sokolov, A. N.; Giebink, N. C., Large bipolaron density at organic semiconductor/electrode interfaces. *Nat Commun* **2017**, *8* (1), 2252.
43. Cao, S.; Low, J.; Yu, J.; Jaroniec, M., Polymeric photocatalysts based on graphitic carbon nitride. *Adv Mater* **2015**, *27* (13), 2150-76.
44. Ong, W. J.; Tan, L. L.; Ng, Y. H.; Yong, S. T.; Chai, S. P., Graphitic Carbon Nitride (g-C₃N₄)-Based Photocatalysts for Artificial Photosynthesis and Environmental Remediation: Are We a Step Closer To Achieving Sustainability? *Chem Rev* **2016**, *116* (12), 7159-329.
45. Zhou, Z.; Zhang, Y.; Shen, Y.; Liu, S., Molecular engineering of polymeric carbon nitride: advancing applications from photocatalysis to biosensing and more. *Chem Soc Rev* **2018**, *47* (7), 2298-2321.
46. Wang, Y.; Vogel, A.; Sachs, M.; Sprick, R. S.; Wilbraham, L.; Moniz, S. J.; Godin, R.; Zwiijnenburg, M. A.; Durrant, J. R.; Cooper, A. I., Current understanding and challenges of solar-driven hydrogen generation using polymeric photocatalysts. *Nature Energy* **2019**, 1-15.
47. Ghosh, I.; Khamrai, J.; Savateev, A.; Shlapakov, N.; Antonietti, M.; König, B., Organic semiconductor photocatalyst can bifunctionalize arenes and heteroarenes. *Science* **2019**, *365* (6451), 360-366.
48. Zhang, G.; Lin, L.; Li, G.; Zhang, Y.; Savateev, A.; Zafeiratos, S.; Wang, X.; Antonietti, M., Ionothermal Synthesis of Triazine-Heptazine-Based Copolymers with Apparent Quantum Yields of 60 % at 420 nm for Solar Hydrogen Production from "Sea Water". *Angew Chem Int Ed Engl* **2018**, *57* (30), 9372-9376.
49. Han, Q.; Cheng, Z.; Wang, B.; Zhang, H.; Qu, L., Significant Enhancement of Visible-Light-Driven Hydrogen Evolution by Structure Regulation of Carbon Nitrides. *ACS Nano* **2018**, *12* (6), 5221-5227.
50. Bojdys, M. J.; Müller, J. O.; Antonietti, M.; Thomas, A., Ionothermal synthesis of crystalline, condensed, graphitic carbon nitride. *Chemistry* **2008**, *14* (27), 8177-82.
51. Wang, X.; Maeda, K.; Thomas, A.; Takanabe, K.; Xin, G.; Carlsson, J. M.; Domen, K.; Antonietti, M., A metal-free polymeric photocatalyst for hydrogen production from water under visible light. *Nat Mater* **2009**, *8* (1), 76-80.

52. Kuriki, R.; Ishitani, O.; Maeda, K., Unique Solvent Effects on Visible-Light CO₂ Reduction over Ruthenium(II)-Complex/Carbon Nitride Hybrid Photocatalysts. *ACS Appl Mater Interfaces* **2016**, *8* (9), 6011-8.
53. Cui, Y.; Ding, Z.; Liu, P.; Antonietti, M.; Fu, X.; Wang, X., Metal-free activation of H₂O₂ by g-C₃N₄ under visible light irradiation for the degradation of organic pollutants. *Phys Chem Chem Phys* **2012**, *14* (4), 1455-62.
54. Qin, Y.; Martindale, B. C.; Sun, R.; Rieth, A. J.; Nocera, D. G., Solar-driven tandem photoredox nickel-catalysed cross-coupling using modified carbon nitride. *Chemical Science* **2020**, *11* (28), 7456-7461.
55. Rieth, A. J.; Qin, Y.; Martindale, B. C.; Nocera, D. G., Long-Lived Triplet Excited State in a Heterogeneous Modified Carbon Nitride Photocatalyst. *Journal of the American Chemical Society* **2021**.
56. Xu, J.; Zhang, L.; Shi, R.; Zhu, Y., Chemical exfoliation of graphitic carbon nitride for efficient heterogeneous photocatalysis. *Journal of Materials Chemistry A* **2013**, *1* (46), 14766-14772.
57. Lau, V. W. H.; Yu, V. W. Z.; Ehrat, F.; Botari, T.; Moudrakovski, I.; Simon, T.; Duppel, V.; Medina, E.; Stolarczyk, J. K.; Feldmann, J.; Blum, V.; Lotsch, B. V., Urea-Modified Carbon Nitrides: Enhancing Photocatalytic Hydrogen Evolution by Rational Defect Engineering. *Advanced Energy Materials* **2017**, *7* (12).
58. Ishida, Y.; Chabanne, L.; Antonietti, M.; Shalom, M., Morphology control and photocatalysis enhancement by the one-pot synthesis of carbon nitride from preorganized hydrogen-bonded supramolecular precursors. *Langmuir* **2014**, *30* (2), 447-51.
59. Li, X.-H.; Zhang, J.; Chen, X.; Fischer, A.; Thomas, A.; Antonietti, M.; Wang, X., Condensed graphitic carbon nitride nanorods by nanoconfinement: promotion of crystallinity on photocatalytic conversion. *Chemistry of Materials* **2011**, *23* (19), 4344-4348.
60. Wang, W.; Yu, J. C.; Shen, Z.; Chan, D. K.; Gu, T., g-C₃N₄ quantum dots: direct synthesis, upconversion properties and photocatalytic application. *Chem Commun (Camb)* **2014**, *50* (70), 10148-50.
61. Jiang, L.; Yuan, X.; Pan, Y.; Liang, J.; Zeng, G.; Wu, Z.; Wang, H., Doping of graphitic carbon nitride for photocatalysis: a review. *Applied Catalysis B: Environmental* **2017**, *217*, 388-406.
62. Lau, V. W.; Moudrakovski, I.; Botari, T.; Weinberger, S.; Mesch, M. B.; Duppel, V.; Senker, J.; Blum, V.; Lotsch, B. V., Rational design of carbon nitride photocatalysts by identification of cyanamide defects as catalytically relevant sites. *Nat Commun* **2016**, *7*, 12165.
63. Schlomberg, H.; Kröger, J.; Savasci, G.; Terban, M. W.; Bette, S.; Moudrakovski, I.; Duppel, V.; Podjaski, F.; Siegel, R.; Senker, J.; Dinnebier, R. E.; Ochsenfeld, C.; Lotsch, B. V., Structural Insights into Poly(Heptazine Imides): A Light-Storing Carbon Nitride Material for Dark Photocatalysis. *Chem Mater* **2019**, *31* (18), 7478-7486.

64. Godin, R.; Wang, Y.; Zwijnenburg, M. A.; Tang, J.; Durrant, J. R., Time-Resolved Spectroscopic Investigation of Charge Trapping in Carbon Nitrides Photocatalysts for Hydrogen Generation. *J Am Chem Soc* **2017**, *139* (14), 5216-5224.
65. Kasap, H.; Caputo, C. A.; Martindale, B. C.; Godin, R.; Lau, V. W.; Lotsch, B. V.; Durrant, J. R.; Reisner, E., Solar-Driven Reduction of Aqueous Protons Coupled to Selective Alcohol Oxidation with a Carbon Nitride-Molecular Ni Catalyst System. *J Am Chem Soc* **2016**, *138* (29), 9183-92.
66. Yang, W.; Godin, R.; Kasap, H.; Moss, B.; Dong, Y.; Hillman, S. A. J.; Steier, L.; Reisner, E.; Durrant, J. R., Electron Accumulation Induces Efficiency Bottleneck for Hydrogen Production in Carbon Nitride Photocatalysts. *J Am Chem Soc* **2019**, *141* (28), 11219-11229.
67. Zhang, G.; Li, G.; Lan, Z. A.; Lin, L.; Savateev, A.; Heil, T.; Zafeirotos, S.; Wang, X.; Antonietti, M., Optimizing optical absorption, exciton dissociation, and charge transfer of a polymeric carbon nitride with ultrahigh solar hydrogen production activity. *Angewandte Chemie* **2017**, *129* (43), 13630-13634.
68. Zhang, G.; Savateev, A.; Zhao, Y.; Li, L.; Antonietti, M., Advancing the $n \rightarrow \pi^*$ electron transition of carbon nitride nanotubes for H₂ photosynthesis. *Journal of Materials Chemistry A* **2017**, *5* (25), 12723-12728.
69. Savateev, A.; Tarakina, N. V.; Strauss, V.; Hussain, T.; Ten Brummelhuis, K.; Sánchez Vadillo, J. M.; Markushyna, Y.; Mazzanti, S.; Tyutyunnik, A. P.; Walczak, R.; Oschatz, M.; Guldi, D. M.; Karton, A.; Antonietti, M., Potassium Poly(Heptazine Imide): Transition Metal-Free Solid-State Triplet Sensitizer in Cascade Energy Transfer and [3+2]-cycloadditions. *Angew Chem Int Ed Engl* **2020**.
70. Niu, P.; Yin, L. C.; Yang, Y. Q.; Liu, G.; Cheng, H. M., Increasing the visible light absorption of graphitic carbon nitride (Melon) photocatalysts by homogeneous self-modification with nitrogen vacancies. *Advanced Materials* **2014**, *26* (47), 8046-8052.
71. Chen, Y.; Wang, B.; Lin, S.; Zhang, Y.; Wang, X., Activation of $n \rightarrow \pi^*$ transitions in two-dimensional conjugated polymers for visible light photocatalysis. *The Journal of Physical Chemistry C* **2014**, *118* (51), 29981-29989.
72. Su, F.-Y.; Xu, C.-Q.; Yu, Y.-X.; Zhang, W.-D., Carbon self-doping induced activation of $n-\pi^*$ electronic transitions of g-C₃N₄ nanosheets for efficient photocatalytic H₂ evolution. *ChemCatChem* **2016**, *8* (22), 3527-3535.
73. Xue, J.; Fujitsuka, M.; Majima, T., The role of nitrogen defects in graphitic carbon nitride for visible-light-driven hydrogen evolution. *Physical Chemistry Chemical Physics* **2019**, *21* (5), 2318-2324.
74. Azofra, L. M.; MacFarlane, D. R.; Sun, C., A DFT study of planar vs. corrugated graphene-like carbon nitride (gC₃N₄) and its role in the catalytic performance of CO₂ conversion. *Physical Chemistry Chemical Physics* **2016**, *18* (27), 18507-18514.

75. Ullah, N.; Chen, S.; Zhao, Y.; Zhang, R., Photoinduced Water-Heptazine Electron-Driven Proton Transfer: Perspective for Water Splitting with g-C. *J Phys Chem Lett* **2019**, *10*(15), 4310-4316.
76. Ma, H.; Zhang, X.; Jin, F.; Zhou, H.; Zhang, J.; Ma, Y., Crucial roles of triazinic-N=O and C=O groups in photocatalytic water splitting on graphitic carbon nitride. *Journal of Materials Chemistry A* **2021**, *9*(9), 5522-5532.
77. You, P.; Lian, C.; Chen, D.; Xu, J.; Zhang, C.; Meng, S.; Wang, E., Nonadiabatic Dynamics of Photocatalytic Water Splitting on A Polymeric Semiconductor. *Nano Letters* **2021**, DOI: 10.1021/acs.nanolett.1c01187.
78. Wei, W.; Jacob, T., Strong excitonic effects in the optical properties of graphitic carbon nitride g-C₃N₄ from first principles. *Physical Review B* **2013**, *87*(8), 085202.
79. Rahman, M. Z.; Mullins, C. B., Understanding Charge Transport in Carbon Nitride for Enhanced Photocatalytic Solar Fuel Production. *Acc Chem Res* **2019**, *52*(1), 248-257.
80. Butchosa, C.; Guiglion, P.; Zwiijnenburg, M. A., Carbon Nitride Photocatalysts for Water Splitting: A Computational Perspective. *The Journal of Physical Chemistry C* **2014**, *118*(43), 24833-24842.
81. Srinivasu, K.; Modak, B.; Ghosh, S. K., Porous graphitic carbon nitride: a possible metal-free photocatalyst for water splitting. *The Journal of Physical Chemistry C* **2014**, *118*(46), 26479-26484.
82. Melissen, S.; Le Bahers, T.; Steinmann, S. N.; Sautet, P., Relationship between carbon nitride structure and exciton binding energies: a DFT perspective. *The Journal of Physical Chemistry C* **2015**, *119*(45), 25188-25196.
83. Liu, N.; Li, T.; Zhao, Z.; Liu, J.; Luo, X.; Yuan, X.; Luo, K.; He, J.; Yu, D.; Zhao, Y., From Triazine to Heptazine: Origin of Graphitic Carbon Nitride as a Photocatalyst. *ACS Omega* **2020**, *5*(21), 12557-12567.
84. Domcke, W.; Sobolewski, A. L.; Schlenker, C. W., Photooxidation of water with heptazine-based molecular photocatalysts: Insights from spectroscopy and computational chemistry. *J Chem Phys* **2020**, *153*(10), 100902.
85. Domcke, W.; Ehrmaier, J.; Sobolewski, A. L., Solar Energy Harvesting with Carbon Nitrides and N-Heterocyclic Frameworks: Do We Understand the Mechanism? *ChemPhotoChem* **2019**, *3*(1), 10-23.
86. Audebert, P.; Kroke, E.; Posern, C.; Lee, S. H., State of the Art in the Preparation and Properties of Molecular Monomeric. *Chem Rev* **2021**, *121*(4), 2515-2544.
87. Merschjann, C.; Tyborski, T.; Orthmann, S.; Yang, F.; Schwarzburg, K.; Lublow, M.; Lux-Steiner, M.-C.; Schedel-Niedrig, T., Photophysics of polymeric carbon nitride: An optical quasimonomer. *Physical Review B* **2013**, *87*(20), 205204.

88. Ehrmaier, J.; Karsili, T. N. V.; Sobolewski, A. L.; Domcke, W., Mechanism of Photocatalytic Water Splitting with Graphitic Carbon Nitride: Photochemistry of the Heptazine-Water Complex. *J Phys Chem A* **2017**, *121* (25), 4754-4764.
89. Schlenker, C. W.; Thompson, M. E., The molecular nature of photovoltage losses in organic solar cells. *Chemical communications* **2011**, *47* (13), 3702-3716.
90. Ren, G.; Schlenker, C. W.; Ahmed, E.; Subramaniyan, S.; Olthof, S.; Kahn, A.; Ginger, D. S.; Jenekhe, S. A., Photoinduced hole transfer becomes suppressed with diminished driving force in polymer-fullerene solar cells while electron transfer remains active. *Advanced Functional Materials* **2013**, *23* (10), 1238-1249.
91. Rabe, E. J.; Schlenker, C. W., Excited-state Energies Drive Charge-transfer in Organic Semiconductors. In *World Scientific Handbook of ORGANIC OPTOELECTRONIC DEVICES: Volume 2-Organic Photovoltaics (OPVs)*, World Scientific: 2018; pp 89-120.
92. Armstrong, D. A.; Huie, R. E.; Koppenol, W. H.; Lyman, S. V.; Merényi, G.; Neta, P.; Ruscic, B.; Stanbury, D. M.; Steenken, S.; Wardman, P., Standard electrode potentials involving radicals in aqueous solution: inorganic radicals (IUPAC Technical Report). *Pure and Applied Chemistry* **2015**, *87* (11-12), 1139-1150.
93. Rabe, E. J.; Corp, K. L.; Huang, X.; Ehrmaier, J.; Flores, R. G.; Estes, S. L.; Sobolewski, A. L.; Domcke, W.; Schlenker, C. W., Barrierless Heptazine-Driven Excited State Proton-Coupled Electron Transfer: Implications for Controlling Photochemistry of Carbon Nitrides and Aza-Arenes. *The Journal of Physical Chemistry C* **2019**, *123* (49), 29580-29588.
94. Viswanathan, V.; Hansen, H. A.; Nørskov, J. K., Selective Electrochemical Generation of Hydrogen Peroxide from Water Oxidation. *J Phys Chem Lett* **2015**, *6* (21), 4224-8.
95. Siahrostami, S.; Li, G. L.; Viswanathan, V.; Nørskov, J. K., One- or Two-Electron Water Oxidation, Hydroxyl Radical, or H₂O₂. *J Phys Chem Lett* **2017**, *8* (6), 1157-1160.
96. Shi, X.; Siahrostami, S.; Li, G. L.; Zhang, Y.; Chakthranont, P.; Studt, F.; Jaramillo, T. F.; Zheng, X.; Nørskov, J. K., Understanding activity trends in electrochemical water oxidation to form hydrogen peroxide. *Nat Commun* **2017**, *8* (1), 701.
97. Baek, J. H.; Gill, T. M.; Abroshan, H.; Park, S.; Shi, X.; Nørskov, J.; Jung, H. S.; Siahrostami, S.; Zheng, X., Selective and Efficient Gd-Doped BiVO₄ Photoanode for Two-Electron Water Oxidation to H₂O₂. *ACS Energy Letters* **2019**, *4* (3), 720-728.
98. Weber, F.; Tremblay, J. C.; Bande, A., Proton-Coupled Electron-Transfer Dynamics of Water Oxidation at N-Doped Graphene Oxides. *The Journal of Physical Chemistry C* **2020**.
99. Sobolewski, A. L.; Domcke, W., Photoinduced water splitting with oxotitanium porphyrin: a computational study. *Phys Chem Chem Phys* **2012**, *14* (37), 12807-17.

100. Yamamoto, K.; Takatsuka, K., On the photocatalytic cycle of water splitting with small manganese oxides and the roles of water clusters as direct sources of oxygen molecules. *Phys Chem Chem Phys* **2018**, *20* (9), 6708-6725.
101. Li, X.; Hartley, G.; Ward, A. J.; Young, P. A.; Masters, A. F.; Maschmeyer, T., Hydrogenated defects in graphitic carbon nitride nanosheets for improved photocatalytic hydrogen evolution. *The Journal of Physical Chemistry C* **2015**, *119* (27), 14938-14946.
102. Corp, K. L.; Schlenker, C. W., Ultrafast Spectroscopy Reveals Electron-Transfer Cascade That Improves Hydrogen Evolution with Carbon Nitride Photocatalysts. *J Am Chem Soc* **2017**, *139* (23), 7904-7912.
103. Köhler, A.; Bässler, H., *Electronic processes in organic semiconductors: An introduction*. John Wiley & Sons: 2015.
104. Ruckebusch, C.; Sliwa, M.; Pernot, P. d.; De Juan, A.; Tauler, R., Comprehensive data analysis of femtosecond transient absorption spectra: A review. *Journal of Photochemistry and Photobiology C: Photochemistry Reviews* **2012**, *13* (1), 1-27.
105. Snellenburg, J.; Laptinok, S.; Seger, R.; Mullen, K.; Van Stokkum, I., Glotaran: A Java-based graphical user interface for the R package TIMP. **2012**.
106. Wang, Y.; Wang, X.; Antonietti, M., Polymeric graphitic carbon nitride as a heterogeneous organocatalyst: from photochemistry to multipurpose catalysis to sustainable chemistry. *Angewandte Chemie International Edition* **2012**, *51* (1), 68-89.
107. Wang, X. L.; Fang, W. Q.; Liu, W.; Jia, Y.; Jing, D.; Wang, Y.; Yang, L.-Y.; Gong, X.-Q.; Yao, Y.-F.; Yang, H. G., Brønsted base site engineering of graphitic carbon nitride for enhanced photocatalytic activity. *Journal of Materials Chemistry A* **2017**, *5* (36), 19227-19236.
108. Niu, P.; Qiao, M.; Li, Y.; Huang, L.; Zhai, T., Distinctive defects engineering in graphitic carbon nitride for greatly extended visible light photocatalytic hydrogen evolution. *Nano Energy* **2018**, *44*, 73-81.
109. Wang, C.; Wan, Q.; Cheng, J.; Lin, S.; Savateev, A.; Antonietti, M.; Wang, X., Efficient aerobic oxidation of alcohols to esters by acidified carbon nitride photocatalysts. *Journal of Catalysis* **2021**, *393*, 116-125.
110. Lau, V. W.; Mesch, M. B.; Duppel, V.; Blum, V.; Senker, J.; Lotsch, B. V., Low-molecular-weight carbon nitrides for solar hydrogen evolution. *J Am Chem Soc* **2015**, *137* (3), 1064-72.
111. Kumar, S.; Sharma, N.; Kailasam, K., Emergence of s-heptazines: from trichloro-s-heptazine building blocks to functional materials. *Journal of Materials Chemistry A* **2018**, *6* (44), 21719-21728.

112. Zheng, J.-F.; Xie, Z.-P.; Li, Z.; Chen, Y.; Fang, X.; Chen, X.; Lin, M.-J., Structural design of small-molecule carbon-nitride dyes for photocatalytic hydrogen evolution. *Dyes and Pigments* **2021**, *185*, 108946.
113. Rabe, E. J.; Corp, K. L.; Sobolewski, A. L.; Domcke, W.; Schlenker, C. W., Proton-Coupled Electron Transfer from Water to a Model Heptazine-Based Molecular Photocatalyst. *J Phys Chem Lett* **2018**, *9*(21), 6257-6261.
114. Flom, S. R.; Barbara, P. F., Proton transfer and hydrogen bonding in the internal conversion of S1 anthraquinones. *The Journal of Physical Chemistry* **1985**, *89*(21), 4489-4494.
115. Han, G. R.; Hwang, D.; Lee, S.; Lee, J. W.; Lim, E.; Heo, J.; Kim, S. K., Shedding new light on an old molecule: quinophthalone displays uncommon N-to-O excited state intramolecular proton transfer (ESIPT) between photobases. *Sci Rep* **2017**, *7*(1), 3863.
116. Liu, J.; Liu, Y.; Liu, N.; Han, Y.; Zhang, X.; Huang, H.; Lifshitz, Y.; Lee, S.-T.; Zhong, J.; Kang, Z., Metal-free efficient photocatalyst for stable visible water splitting via a two-electron pathway. *Science* **2015**, *347*(6225), 970-974.
117. Corp, K. L.; Rabe, E. J.; Huang, X.; Ehrmaier, J.; Kaiser, M. E.; Sobolewski, A. L.; Domcke, W.; Schlenker, C. W., Control of Excited-State Proton-Coupled Electron Transfer by Ultrafast Pump-Push-Probe Spectroscopy in Heptazine-Phenol Complexes: Implications for Photochemical Water Oxidation. *The Journal of Physical Chemistry C* **2020**, *124*(17), 9151-9160.
118. Dongare, P.; Bonn, A. G.; Maji, S.; Hammarström, L., Analysis of Hydrogen-Bonding Effects on Excited-State Proton-Coupled Electron Transfer from a Series of Phenols to a Re (I) Polypyridyl Complex. *The Journal of Physical Chemistry C* **2017**, *121*(23), 12569-12576.
119. Lakowicz, J. R., *Principles of fluorescence spectroscopy*. Springer science & business media: 2013.
120. Rabe, E. J.; Goldwyn, H. J.; Hwang, D.; Masiello, D. J.; Schlenker, C. W., Intermolecular Hydrogen Bonding Tunes Vibronic Coupling in Heptazine Complexes. *J Phys Chem B* **2020**.
121. Bronner, C.; Wenger, O. S., Kinetic isotope effects in reductive excited-state quenching of Ru (2, 2'-bipyrazine) 32+ by phenols. *The Journal of Physical Chemistry Letters* **2012**, *3*(1), 70-74.
122. Yamaji, M.; Oshima, J.; Hidaka, M., Verification of the electron/proton coupled mechanism for phenolic H-atom transfer using a triplet π , π^* carbonyl. *Chemical Physics Letters* **2009**, *475*(4-6), 235-239.
123. Warren, J. J.; Tronic, T. A.; Mayer, J. M., Thermochemistry of proton-coupled electron transfer reagents and its implications. *Chem Rev* **2010**, *110*(12), 6961-7001.
124. de Jong, M.; Seijo, L.; Meijerink, A.; Rabouw, F. T., Resolving the ambiguity in the relation between Stokes shift and Huang-Rhys parameter. *Phys Chem Chem Phys* **2015**, *17*(26), 16959-69.

125. Baessler, H.; Schweitzer, B., Site-selective fluorescence spectroscopy of conjugated polymers and oligomers. *Accounts of Chemical Research* **1999**, *32* (2), 173-182.
126. Huang, K.; Rhys, A., Theory of light absorption and non-radiative transitions in F-centres. *Proceedings of the Royal Society of London. Series A. Mathematical and Physical Sciences* **1950**, *204* (1078), 406-423.
127. Hansch, C.; Leo, A.; Taft, R., A survey of Hammett substituent constants and resonance and field parameters. *Chemical reviews* **1991**, *91* (2), 165-195.
128. Liu, Y. H.; Wang, S. M.; Wang, C. W.; Zhu, C.; Han, K. L.; Lin, S. H., Orientation hydrogen-bonding effect on vibronic spectra of isoquinoline in water solvent: Franck-Condon simulation and interpretation. *J Chem Phys* **2016**, *145* (16), 164314.
129. Yan, X.; Zhang, H.; Cai, W.; Zhao, A.; Wang, J.; Shen, W., Effects of intramolecular hydrogen bonds on phosphorescence emission: A theoretical perspective. *Applied Organometallic Chemistry* **2020**, *34* (4), e5527.
130. Dierksen, M.; Grimme, S., Density functional calculations of the vibronic structure of electronic absorption spectra. *J Chem Phys* **2004**, *120* (8), 3544-54.
131. Karpovich, D.; Blanchard, G., Relating the polarity-dependent fluorescence response of pyrene to vibronic coupling. Achieving a fundamental understanding of the py polarity scale. *The Journal of Physical Chemistry* **1995**, *99* (12), 3951-3958.
132. Mastroph, H.; Towns, A., Fine Structure in Electronic Spectra of Cyanine Dyes: Are Sub-Bands Largely Determined by a Dominant Vibration or a Collection of Singly Excited Vibrations? *Chemphyschem* **2018**, *19* (9), 1016-1023.
133. Liu, X.; Sobolewski, A. L.; Borrelli, R.; Domcke, W., Computational investigation of the photoinduced homolytic dissociation of water in the pyridine-water complex. *Phys Chem Chem Phys* **2013**, *15* (16), 5957-66.
134. Ehrmaier, J.; Janicki, M. J.; Sobolewski, A. L.; Domcke, W., Mechanism of photocatalytic water splitting with triazine-based carbon nitrides: insights from ab initio calculations for the triazine-water complex. *Phys Chem Chem Phys* **2018**, *20* (21), 14420-14430.
135. Liu, X.; Karsili, T. N.; Sobolewski, A. L.; Domcke, W., Photocatalytic Water Splitting with the Acridine Chromophore: A Computational Study. *J Phys Chem B* **2015**, *119* (33), 10664-72.
136. Bakulin, A. A.; Rao, A.; Pavelyev, V. G.; van Loosdrecht, P. H.; Pshenichnikov, M. S.; Niedzialek, D.; Cornil, J.; Beljonne, D.; Friend, R. H., The role of driving energy and delocalized States for charge separation in organic semiconductors. *Science* **2012**, *335* (6074), 1340-4.
137. Kee, T. W., Femtosecond Pump-Push-Probe and Pump-Dump-Probe Spectroscopy of Conjugated Polymers: New Insight and Opportunities. *J Phys Chem Lett* **2014**, *5* (18), 3231-40.

138. Lim, S. S.; Giovanni, D.; Zhang, Q.; Solanki, A.; Jamaludin, N. F.; Lim, J. W. M.; Mathews, N.; Mhaisalkar, S.; Pshenichnikov, M. S.; Sum, T. C., Hot carrier extraction in CH. *Sci Adv* **2019**, *5* (11), eaax3620.
139. Lin, S.; Huang, H.; Ma, T.; Zhang, Y., Photocatalytic Oxygen Evolution from Water Splitting. *Advanced Science* **2020**, 2002458.
140. Balzani, V.; Moggi, L.; Manfrin, M. F.; Bolletta, F.; Gleria, M., Solar Energy Conversion by Water Photodissociation: Transition metal complexes can provide low-energy cyclic systems for catalytic photodissociation of water. *Science* **1975**, *189*(4206), 852-6.
141. Nosaka, Y.; Nosaka, A., Understanding hydroxyl radical (\bullet OH) generation processes in photocatalysis. *ACS Energy Letters* **2016**, *1*(2), 356-359.
142. Maier, A. C.; Iglebaek, E. H.; Jonsson, M., Confirming the formation of hydroxyl radicals in the catalytic decomposition of H₂O₂ on metal oxides using coumarin as a probe. *ChemCatChem* **2019**, *11* (22), 5435-5438.
143. Ehrmaier, J.; Rabe, E. J.; Pristash, S. R.; Corp, K. L.; Schlenker, C. W.; Sobolewski, A. L.; Domcke, W., Singlet-Triplet Inversion in Heptazine and in Polymeric Carbon Nitrides. *J Phys Chem A* **2019**, *123*(38), 8099-8108.
144. Kollmar, H.; Staemmler, V., Violation of Hund's rule by spin polarization in molecules. *Theoretica chimica acta* **1978**, *48*(3), 223-239.
145. Koseki, S.; Nakajima, T.; Toyota, A., Violation of Hund's multiplicity rule in the electronically excited states of conjugated hydrocarbons. *Can. J. Chem.* **1985**, *63*(7), 1572-1579.
146. Englman, R.; Jortner, J., The energy gap law for radiationless transitions in large molecules. *Molecular Physics* **1970**, *18*(2), 145-164.
147. Ehrmaier, J.; Huang, X.; Rabe, E. J.; Corp, K. L.; Schlenker, C. W.; Sobolewski, A. L.; Domcke, W., Molecular Design of Heptazine-Based Photocatalysts: Effect of Substituents on Photocatalytic Efficiency and Photostability. *J Phys Chem A* **2020**, *124*(19), 3698-3710.
148. Samanta, S.; Srivastava, R., Catalytic conversion of CO₂ to chemicals and fuels: the collective thermocatalytic/photocatalytic/electrocatalytic approach with graphitic carbon nitride. *Materials Advances* **2020**, *1*(6), 1506-1545.
149. Liu, R.; Chen, Z.; Yao, Y.; Li, Y.; Cheema, W. A.; Wang, D.; Zhu, S., Recent advancements in gC₃N₄-based photocatalysts for photocatalytic CO₂ reduction: a mini review. *RSC Advances* **2020**, *10* (49), 29408-29418.
150. Lu, Q.; Eid, K.; Li, W.; Abdullah, A. M.; Xu, G.; Varma, R. S., Engineering Graphitic Carbon Nitride (g-C₃N₄) for Catalytic Reduction of CO₂ to Fuels and Chemicals: Strategy and Mechanism. *Green Chemistry* **2021**.

151. Ehrmaier, J.; Sobolewski, A. L.; Domcke, W., Role of the pyridinyl radical in the light-driven reduction of carbon dioxide: a first-principles study. *The Journal of Physical Chemistry A* **2019**, *123* (17), 3678-3684.
152. Qin, J.; Wang, S.; Ren, H.; Hou, Y.; Wang, X., Photocatalytic reduction of CO₂ by graphitic carbon nitride polymers derived from urea and barbituric acid. *Applied Catalysis B: Environmental* **2015**, *179*, 1-8.
153. Fu, J.; Zhu, B.; Jiang, C.; Cheng, B.; You, W.; Yu, J., Hierarchical porous O-doped g-C₃N₄ with enhanced photocatalytic CO₂ reduction activity. *Small* **2017**, *13* (15), 1603938.
154. Yang, P.; Zhuzhang, H.; Wang, R.; Lin, W.; Wang, X., Carbon vacancies in a melon polymeric matrix promote photocatalytic carbon dioxide conversion. *Angewandte Chemie International Edition* **2019**, *58* (4), 1134-1137.
155. Li, H.; Zhu, B.; Cao, S.; Yu, J., Controlling defects in crystalline carbon nitride to optimize photocatalytic CO₂ reduction. *Chemical Communications* **2020**, *56* (42), 5641-5644.
156. Zheng, X.; Yu, P.; Wang, J., Ultrafast intramolecular vibrational energy transfer in carbon nitride hydrocolloid examined by femtosecond two-dimensional infrared spectroscopy. *The Journal of chemical physics* **2019**, *150* (19), 194703.
157. Muñoz-Batista, M. J.; Nasalevich, M. A.; Savenije, T. J.; Kapteijn, F.; Gascon, J.; Kubacka, A.; Fernández-García, M., Enhancing promoting effects in g-C₃N₄-Mn⁺/CeO₂-TiO₂ ternary composites: Photo-handling of charge carriers. *Applied Catalysis B: Environmental* **2015**, *176*, 687-698.
158. Capobianco, M. D.; Pattengale, B.; Neu, J.; Schmuttenmaer, C. A., Single Copper Atoms Enhance Photoconductivity in g-C₃N₄. *The Journal of Physical Chemistry Letters* **2020**, *11* (20), 8873-8879.